

8-2015

Performance analysis of a Copper II Sulfate Pentahydrate based thermogalvanic cell.

Steffen Krebs
University of Louisville

Follow this and additional works at: <https://ir.library.louisville.edu/etd>

Part of the [Mechanical Engineering Commons](#)

Recommended Citation

Krebs, Steffen, "Performance analysis of a Copper II Sulfate Pentahydrate based thermogalvanic cell." (2015). *Electronic Theses and Dissertations*. Paper 2215.
<https://doi.org/10.18297/etd/2215>

This Master's Thesis is brought to you for free and open access by ThinkIR: The University of Louisville's Institutional Repository. It has been accepted for inclusion in Electronic Theses and Dissertations by an authorized administrator of ThinkIR: The University of Louisville's Institutional Repository. This title appears here courtesy of the author, who has retained all other copyrights. For more information, please contact thinkir@louisville.edu.

PERFORMANCE ANALYSIS OF A COPPER II SULFATE PENTAHYDRATE
BASED THERMOGALVANIC CELL

By

Steffen Krebs
B.S., Georgetown College, 2013

A Thesis
Submitted to the Faculty of the
J. B. Speed School of Engineering of the University of Louisville
in Partial Fulfillment of the Requirements
for the Degree of

Master of Science in Mechanical Engineering

Department of Mechanical Engineering
University of Louisville
Louisville, Kentucky

August 2015

PERFORMANCE ANALYSIS OF A COPPER II SULFATE PENTAHYDRATE
BASED THERMOGALVANIC CELL

By

Steffen Krebs
B.S., Georgetown College, 2013

A Thesis Approved on

June 11, 2015

by the following Thesis Committee:

Dr. Sam Park

Dr. Ellen Brehob

Dr. Young Kim

ABSTRACT

PERFORMANCE ANALYSIS OF A COPPER II SULFATE PENTAHYDRATE BASED THERMOGALVANIC CELL

Steffen Krebs

June 11, 2015

Low grade heat recovery systems are more relevant today due to the rising costs in energy and transition to non-fossil fuel energy sources. Thermogalvanic cells show potential due to low cost and scalability. In this study the performance of a Copper II Sulfate Pentahydrate based electrolyte was evaluated. The effects of electrolyte concentration, electrode separation, and electrode surface area were studied experimentally. Conductive heat transfer within the electrolyte was simulated via SolidWorks.

All experimental thermocell testing was conducted to find the maximum power production of a particular cell design. The base cell had a six inch electrode separation with two copper electrodes at each end. Temperature gradients were varied from $\Delta T = 10-50$ °C for all tests. Maximum power production was measured for a 0.3M $\text{CuSO}_4 \cdot 5\text{H}_2\text{O}$ based thermocell with six inch electrode spacing and $A = 0.00244 \text{ m}^2$ electrode surface area at $P_{\text{max}} = 7.45 \text{ } \mu\text{W}$. The relative efficiency was calculated to $\eta_r = 0.00198\%$.

TABLE OF CONTENTS

	PAGE
ABSTRACT.....	III
LIST OF TABLES.....	VI
LIST OF FIGURES.....	VII
I. INTRODUCTION.....	1
A. THERMOELECTRIC DEVICES.....	1
1. <i>Applications of Thermoelectric Devices</i>	3
a. Natural Occurring Low Temperature Heat.....	3
b. Waste Heat.....	4
B. THERMO-ELECTROCHEMICAL CELLS.....	6
C. THERMOELECTRIC EFFECT.....	7
1. <i>Seebeck effect</i>	8
2. <i>Peltier Effect</i>	9
3. <i>Thomson Effect</i>	10
4. <i>Thomson (Kelvin) relationships</i>	11
II. RESEARCH OBJECTIVE.....	13
III. PERFORMANCE OF THE THERMOCELL.....	16
IV. THERMOCELL DESIGN CONSIDERATIONS:.....	19
A. ELECTRODE SPACING.....	20
B. ELECTRODE SIZE EFFECT.....	22
C. EFFECT OF ELECTROLYTE CONCENTRATION.....	22
1. <i>Electrolyte Concentration versus temperature difference effect on the potential difference:</i>	23
2. <i>Electrolyte Concentration vs temperature difference effect on the max power output and power density:</i>	24
D. CELL ORIENTATION EFFECT ON PERFORMANCE.....	24
E. INTERNAL RESISTANCE AS A FACTOR FOR CELL PERFORMANCE.....	25
V. EXPERIMENTAL SETUP AND PROCEDURE.....	27
A. ELECTRODE PRETREATMENT.....	31
B. ELECTROLYTE PREPARATION.....	31
C. THERMOCELL TESTING CYCLES.....	32

1. <i>Open circuit voltage testing</i>	32
2. <i>Discharge testing</i>	34
VI. RESULTS AND DISCUSSION	37
1. <i>Seebeck coefficient dependence on concentration</i>	37
2. <i>Seebeck coefficient dependence on electrode area</i>	39
A. POWER PRODUCTION TESTING/ DISCHARGE CAPABILITIES OF A THERMOCELL	40
1. <i>Characterization of 0.01M Copper II Sulfate Pentahydrate based thermocell</i>	40
2. <i>Characterization of 0.1M Copper II Sulfate Pentahydrate based thermocell</i>	42
3. <i>Characterization of 0.3M Copper II Sulfate Pentahydrate based thermocell</i>	45
4. <i>Characterization of 0.3M Copper II Sulfate Pentahydrate based three inch thermocell</i>	48
5. <i>Characterization of 0.3M Copper II Sulfate Pentahydrate based two inch thermocell</i>	50
6. <i>Characterization of 0.3M Copper II Sulfate Pentahydrate based three inch thermocell with 0.00183 m² electrode surface area</i>	53
7. <i>Characterization of 0.3M Copper II Sulfate Pentahydrate based three inch thermocell with 0.00144 m² electrode surface area</i>	55
8. <i>Power dependence on electrolyte concentration</i>	58
9. <i>Power dependence on electrode spacing</i>	59
10. <i>Power dependence on electrode surface area</i>	62
B. HEAT TRANSFER IN A THERMOGALVANIC CELL	65
1. <i>SolidWorks Simulation of Heat flow</i>	66
a. <i>Initial and Boundary Conditions</i>	67
b. <i>Simulation Results</i>	68
2. <i>Condensation of electrolyte</i>	74
VII. CONCLUSION	77
VIII. RECOMMENDATION	79
REFERENCES	80
APPENDICIES	82
CURRICULUM VITAE	83

LIST OF TABLES

TABLES	PAGE
1. Characterization of 0.01M Copper II Sulfate Pentahydrate based thermocell.....	40
2. Characterization of 0.1M Copper II Sulfate Pentahydrate based thermocell.....	42
3. Characterization of 0.3M Copper II Sulfate Pentahydrate based thermocell.....	44
4. Characterization of 0.3M Copper II Sulfate Pentahydrate based 3 inch thermocell....	47
5. Characterization of 0.3M Copper II Sulfate Pentahydrate based 2 inch thermocell.....	50
6. Characterization of 0.3M Copper II Sulfate Pentahydrate based 3 inch thermocell with 0.00183 m ² electrode surface area.....	52
7. Characterization of 0.3M Copper II Sulfate Pentahydrate based 3 inch thermocell with 00144 m ² electrode surface area.....	55

LIST OF FIGURES

FIGURE	PAGE
Figure 1. Schematic of a Thermoelectric Generator.	2
Figure 2. Schematic of a thermogalvanic cell.	7
Figure 3. Thermocouple (Illustration for Seebeck effect) (Lee, 2010).	8
Figure 4. Schematic diagram for the Peltier effect (Lee, 2010).	9
Figure 5. Schematic diagram for the Thomson effect (Lee, 2010).	11
Figure 6. Seebeck coefficient comparison for different redox couples (deBethune, Licht, & Swendeman, 1959).	19
Figure 7. Effect of electrode separation on thermocell resistance (Mua & Quickenden, 1996).	20
Figure 8. Effect of electrode separation on Power conversion efficiency (Mua & Quickenden, 1996).	21
Figure 9. Concentration Dependence on R_{int} (Tester, 1992).	26
Figure 10. Full electrochemical test cell equipment. Warm electrode is on hot plate and connected to hot air supply stream, Cold electrode can be submersed to a cold water bath.	28
Figure 11. Modified electrochemical test cell equipment with a three inch borosilicate glass tube. Cold electrode is in iced water bath and warm electrode is on hot plate and supplied with hot moist air.	30

Figure 12. Small volume beaker setup with filter paper salt bridge. Warm electrode is on hot plate and cold electrode is at room temperature.	31
Figure 13. Open Circuit Voltage Test from 2/20/2015 with 0.01M CuSO ₄ 5H ₂ O concentration and 6 inch electrode separation.	33
Figure 14. Temperature Difference for Test 02/20/2015 (Fig5.).....	33
Figure 15. Test from 2/26/15 with 0.01M CuSO ₄ 5H ₂ O concentration, 6 inch electrode separation and current discharge steps ranging from 0.1 mA to 0.5 mA (step increase of 0.1 mA) at $\Delta T = 30\text{ }^{\circ}\text{C}$	35
Figure 16. Test from 4/25/2015 with 0.3M CuSO ₄ 5H ₂ O concentration and 6 inch electrode separation, discharging steps from $I = -0.1\text{ mA}$ to $I = -20\text{ mA}$ at $\Delta T = 50\text{ }^{\circ}\text{C}$	36
Figure 17. Experimental results of Seebeck coefficient dependence on concentration testing for Copper (II) Sulfate Pentahydrate with copper electrodes.....	38
Figure 18. Experimental results of Seebeck coefficient dependence on electrode surface area testing for Copper (II) Sulfate Pentahydrate with copper electrodes.	39
Figure 19. IV-Discharge Curve for 0.01M CuSO ₄ 5H ₂ O concentration and electrode separation of 6 in.....	42
Figure 20. IV-Discharge Curve for 0.1M CuSO ₄ 5H ₂ O concentration and electrode separation of 6 in.....	45
Figure 21. IV-Discharge Curve for 0.3M CuSO ₄ 5H ₂ O concentration and electrode separation of 6 in.....	47
Figure 22. IV-Discharge Curve for 0.3M CuSO ₄ 5H ₂ O concentration and electrode separation of 3 in.....	50

Figure 23. IV-Discharge Curve for 0.3M CuSO ₄ 5H ₂ O concentration and electrode separation of 2 in.....	52
Figure 24. IV-Discharge Curve for 0.3M CuSO ₄ 5H ₂ O concentration and electrode separation of 3 in. with electrode surface area of A= 0.00183 m ²	55
Figure 25. IV-Discharge Curve for 0.3M CuSO ₄ 5H ₂ O concentration and electrode separation of 3 in. with electrode surface area of A= 0.00144 m ²	57
Figure 26. Power Output depending on Electrolyte Concentration plotted versus current density (all test cycles were conducted at ΔT=50 °C).....	58
Figure 27. Power dependence on electrode spacing plotted versus current density (all test cycles were conducted at ΔT=50 °C).....	60
Figure 28. Electrode spacing effects on relative efficiency and internal resistance (at P _{max} and ΔT= 50 °C).	61
Figure 29. Power dependence on electrode surface area plotted versus current density (all test cycles were conducted at ΔT=50 °C).	63
Figure 30. Electrode surface area effects on relative efficiency and maximum power output (d= 3 inches and ΔT= 50 °C).	64
Figure 31. Thermal image for 0.3M CuSO ₄ 5H ₂ O based thermocell test with the hot electrode side at T= 60°C and the cold electrode at ambient temperature (T= 23°C).	66
Figure 32. Flow velocities shown on the hot electrode side caused by natural heat convection in the thermocell.....	68
Figure 33. Temperature distribution for the small one centimeter length CuSO ₄ 5H ₂ O thermocell after 1800 seconds.	70

Figure 34. Temperature distribution for the six inch $\text{CuSO}_4 \cdot 5\text{H}_2\text{O}$ thermocell after 1800 seconds.....	72
Figure 35. Temperature distribution cut plot at a) 900sec, b) 1800sec, c) 3600sec, and d) 7200s.....	74
Figure 36. Condensation of electrolyte during testing of 0.01M $\text{CuSO}_4 \cdot 5\text{H}_2\text{O}$ based thermocell.	75

I. INTRODUCTION

A. Thermoelectric Devices

Thermoelectric devices have been studied in the past century but research has tremendously increased within the past 15 years. Besides using it for cooling (Peltier cooler), thermoelectric power generators can be used to recover waste heat energy from various industrial processes and other applications. Low grade heat (temperature less than 130 °C) can be harvested from different industrial sources like solar heating or waste streams of cooling water in a power plant (Rowe, 2006). Additionally, internal combustion engines exhaust pipes could be used to recover waste heat which otherwise would escape freely into the atmosphere.

The U.S. Department of Energy has studied different industrial processes and shown that enormous amounts of thermal energy are available to be recovered (Office of Energy Efficiency and Renewable Energy, 2004). For example, for the average power production process only 25 to 44 % of the thermal energy is used efficiently. Steel and aluminum processing procedures have thermal efficiencies around 50 %. Additionally, automobiles and heavy-duty vehicles waste vast amounts of thermal energy by the use of internal combustion engines (thermal efficiency around 40 %). The previously mentioned values indicate that thermoelectric power generation can have a significant impact on waste-heat recovery power generation.

New discoveries in micro- and nanotechnologies have helped the efficiency of thermoelectric energy generator systems. The following figure shows a schematic of a common system used from thermoelectric energy recovery.

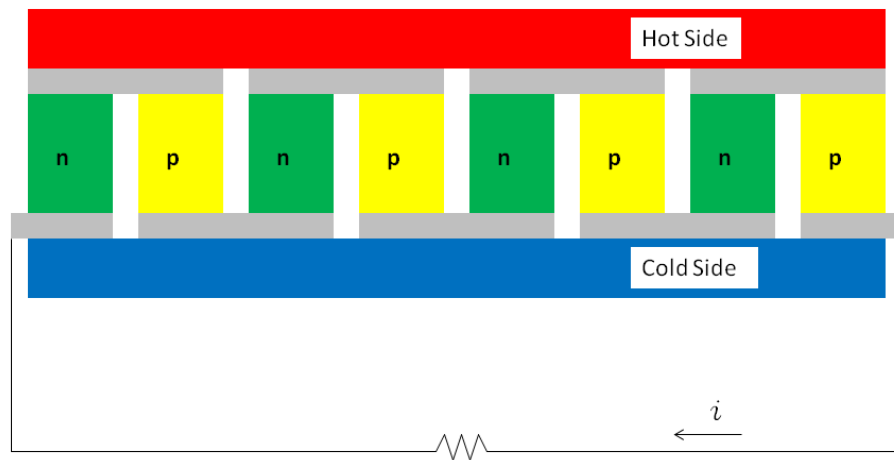


Figure 1. Schematic of a Thermoelectric Generator.

A hot temperature source is positioned on one side of p-type and n-type semiconductor arrangement. P-type semiconductors have an electron deficiency whereas n-type semiconductors have an electron surplus. This combination of semiconductors arranged in an alternating fashion, as seen in Figure 1, allows current flow. A single combination pair of p-type and n-type semiconductors is referred to as a couple.

To effectively compare thermoelectric materials to each other, a thermoelectric figure of merit, sometimes called a ‘goodness factor’, has been introduced:

$$Z = \frac{\alpha^2 \sigma}{\kappa} \quad (1)$$

Here σ is the electrical conductivity, κ represents the total thermal conductivity, and α is the Seebeck coefficient.

1. Applications of Thermoelectric Devices

Thermoelectric power generation has received more attention since crude oil prices increased and climate change is often in the news. Thermoelectric devices are a green technology, totally silent, scalable, and extremely reliable. Especially with free energy input, called waste heat, thermoelectric power generation becomes an extremely attractive source of energy production. Sources of waste heat are electrical systems, industrial processes, or automobile engines. Naturally occurring low heat temperature sources are solar, geothermal, or ocean thermal heat productions (Rowe, 2006) .

a. Natural Occurring Low Temperature Heat

Hot springs or geysers are an easily accessible source of waste heat for thermoelectric power generation. Japan and Iceland have both used hot springs to harvest energy and study geothermal power generation. Generally, natural heat flow within the Earth gives an average temperature gradient of 25 to 30 degrees Celsius per kilometer of depth. Due to inaccessibility and cost few deep drilling projects have been built so far and only easily accessible sources of geothermal heat have been studied. The University of Reykjavik in Iceland has reported a 4 % efficiency for their thermoelectric generator employing a temperature difference of around 75°C (Rowe, 2006).

Ocean thermal energy is another promising source for low heat energy generation. Since 70 % of the earth is covered in water and the average temperature just below the surface is around 4 °C, there is a vast amount of cold water to be used in combination with the surface level water temperature of up to 30 °C. The biggest problem associated with ocean thermal energy conversion is the relatively low temperature gradient which is not favorable for energy extraction.

Solar energy can also be harvested using thermoelectric power generators. A heat collector will absorb light rays from the sun which will produce a temperature gradient between two electrodes. The cold side will be at ambient temperature and electricity will be extracted here. Solar thermoelectric energy conversion can be used in many locations of the earth, favorably in tropical regions, but it also has been used for space applications (Rowe, 2006).

b. Waste Heat

Domestic applications such as heat from a furnace are good applications for waste heat recovery. Heating pipes transporting warm water into radiators can also be used for energy recovery. Household appliances can be used to recover some of the lost thermal energy. For a home heating system using a radiator it is estimated that 5 % of the heat pumped throughout the house can be recovered using thermoelectric modules. This would leave the other 95 % of thermal energy to heat the house.

Steel and metal manufacturing and processing plants use large amounts of cooling water which is discharged to the environment at a constant temperature. Because of this very consistent temperature gradient with its surroundings, these types of processing

plants have great potential for waste heat recovery. The recovered energy could then be used again during subsequent manufacturing and processing of steel (Rowe, 2006).

Internal combustion engines and automobiles in general have received great attention in the recent years for thermoelectric recovery. In 1988 a German university first developed a device to recover thermal energy from exhaust heat (U. Birkholz, 1988). More recently a research team including BMW and Ford integrated a thermoelectric generator into two cars which produced 600 W during vehicle testing (Crane et al., 2013). While this power output is relatively high, it is not enough to sufficiently improve the fuel economy of an automobile. Further improvement is necessary to yield a more satisfactory power output at any road speed.

Another suitable application area for thermoelectric devices is the medical field. Uses vary from external devices like heating or cooling blankets to very sophisticated implantable devices like pacemaker powered by a thermoelectric generator. As thermoelectric devices improve in quality and efficiency their use in medical applications will become more prevalent. However, biocompatibility is a concern for all devices and so materials must be chosen which have previously been established as safe. The wide ranges of applications in the medical field, however, far exceed the additional obstacles that have to be overcome for the use of thermoelectric devices (Rowe, 2006).

Hence another natural continuous source of heat is human body heat. Lowest at night while sleeping and highest during strenuous activities, the temperature difference to ambient is usually around 15 °C. This constant temperature difference can be utilized for energy production using a wristwatch for example. Space and sizing issues are the biggest challenges that have to be overcome to produce consumer products.

B. Thermo-electrochemical cells

Thermoelectric devices for the energy recovery of low-grade heat have been studied in depth over the past decades (Rosi, 1968) to improve their efficiency for widespread use. Their figure of merit, however, is limited and so attention has turned to thermo-electrochemical or thermogalvanic cells.

Thermogalvanic cells have just recently seen a major push in research since other methods of low-grade heat energy conversion have proved to be costly and unreliable, like the Stirling engine (Mancini, 2003). Thermo-electrochemical cells, however, are expected to be a more viable energy source due to their simple design, low maintenance cost while operating continuously, direct energy conversion, and zero carbon emission (Ratkje, 1990).

A thermogalvanic cell makes use of the Seebeck effect, discovered by German physicist Thomas Johann Seebeck in 1821. The corresponding Seebeck coefficient for a given reduction-oxidation (redox) system $B \Leftrightarrow ne^- + A$, is given by,

$$S = \frac{\partial V}{\partial T} = \frac{\Delta S_{B,A}}{nF} \quad (2)$$

where V is the electrode potential, T is the temperature, $\Delta S_{B,A}$ is the reaction entropy for the redox couple, n is the number of electrons, and F is Faraday's constant (Eastman, 1928).

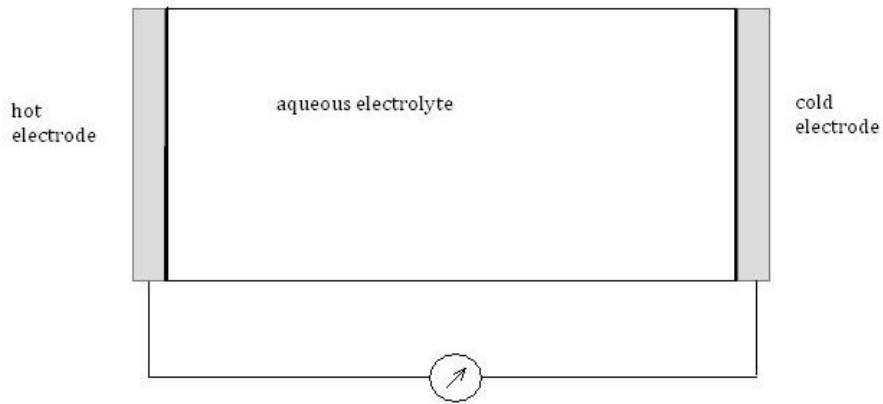


Figure 2. Schematic of a thermogalvanic cell.

The figure above shows the schematic of a thermogalvanic cell. Two electrodes are connected by a liquid electrolyte. The temperature difference between the two electrodes is responsible for the current flow (Seebeck effect).

C. Thermoelectric effect

The thermoelectric effect is the direct conversion of a temperature difference to an electrical current or vice versa. The following effects were discovered independently from each other but are part of the same theory. The thermoelectric effect consists of three effects: the Seebeck effect, the Peltier effect, and the Thomson effect which were discovered in the first half of the 19th century. Thermoelectric effect has a variety of useful applications: generation of electricity, cooling of a secondary device, or measurement of temperature (Lee, 2010).

1. Seebeck effect

The Seebeck effect, discovered by German physicist Thomas Johann Seebeck in 1821, can be easily visualized using a schematic diagram of a thermocouple (device used for temperature measurement).

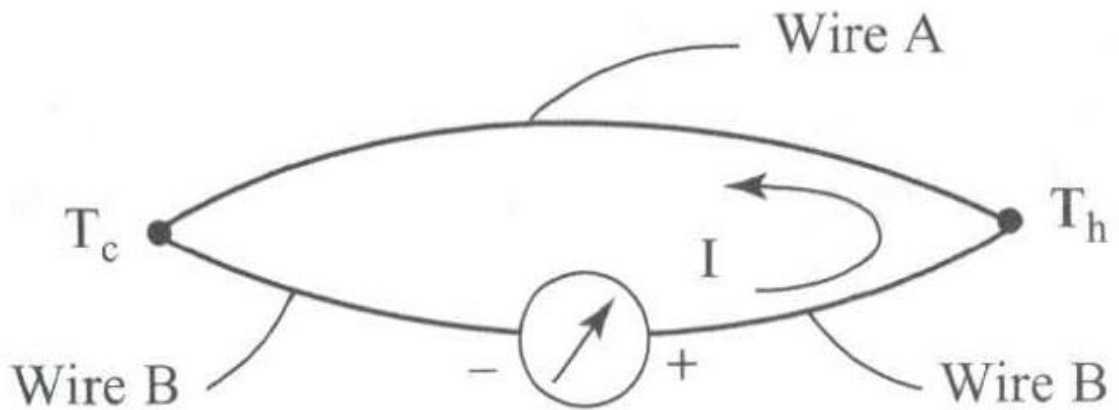


Figure 3. Thermocouple (Illustration for Seebeck effect) (Lee, 2010).

Wire A and Wire B are composed of different materials and the temperature difference is imposed at the two junctions. The temperature difference between the two dissimilar materials creates an electric current. More generally, thermoelectric power generation is the result of a temperature gradient applied across a material. This behavior is called the *Seebeck effect*.

The potential difference between point T_H and T_C is dependent on the temperature difference between T_H and T_C and given by the equation:

$$V = \alpha_{AB} * \Delta T \quad (3)$$

where α is the relative *Seebeck coefficient* with units of [$\mu\text{V}/\text{K}$]. This coefficient can be expressed in terms of absolute Seebeck coefficients in terms of the Seebeck coefficients of each material, A and B, as follows,

$$\alpha_{AB} = \alpha_A - \alpha_B \quad (4)$$

Being a fundamental electronic transport property, the Seebeck coefficient measures the entropy transported by a charge carrier, divided by the charge of the charge carrier (Lee, 2010).

2. Peltier Effect

The Peltier effect, discovered in 1834 by Jean Peltier, is essentially the reverse process of the Seebeck effect. When a potential difference is applied to the thermocouple in Figure 4, a temperature gradient is created between the two wire junctions T_C and T_H . The direction of current flow is responsible for establishing which junction is heated and which junction is cooled. Reversing the current flow will also switch the junction temperatures.

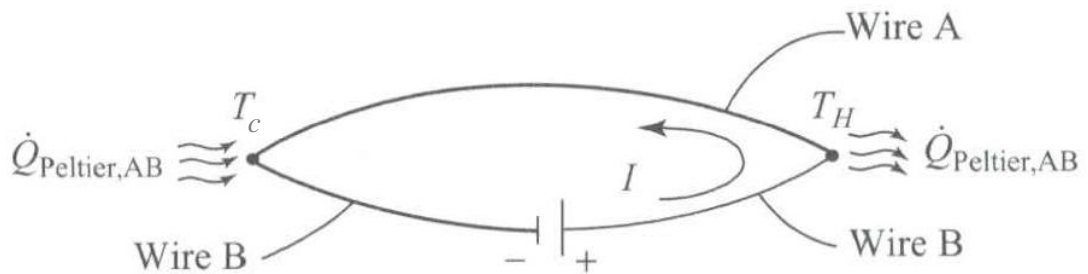


Figure 4. Schematic diagram for the Peltier effect (Lee, 2010).

The rate of Peltier heat dissipated or absorbed is given by,

$$\dot{Q}_{Peltier} = \pi_{AB} * I \quad (5)$$

The sign of $\dot{Q}_{Peltier}$ depends on the direction of the flow of current I and the *Peltier coefficient* π is in units of [W/A] or [V]. The coefficient is a relative coefficient dependent on the wire materials A and B and thus cannot be directly measured. Peltier heating or cooling is a reversible process between heat and electricity. No loss of energy occurs during electricity production and cooling or heating through a voltage difference (Lee, 2010).

3. Thomson Effect

The Thomson effect, named after William Thomson (later Lord Kelvin), discovered in the 1854. When a current flows in a wire with a temperature gradient, heat is either absorbed or dissipated depending on flow direction and material. The amount of Thomson heat, $\dot{Q}_{Thomson}$, given off by a wire is calculated using the following equation.

$$\dot{Q}_{Thomson} = \tau * I * \Delta T \quad (6)$$

τ is the *Thomson coefficient* which indicates if heat is absorbed or dissipated. If τ is positive, then heat is absorbed in Wire A, as seen in Figure 5. Heat is dissipated in Wire B then τ is negative. The Thomson coefficient is unique since it can be measure directly for any material. It is also a reversible process between heat and electricity (Lee, 2010).

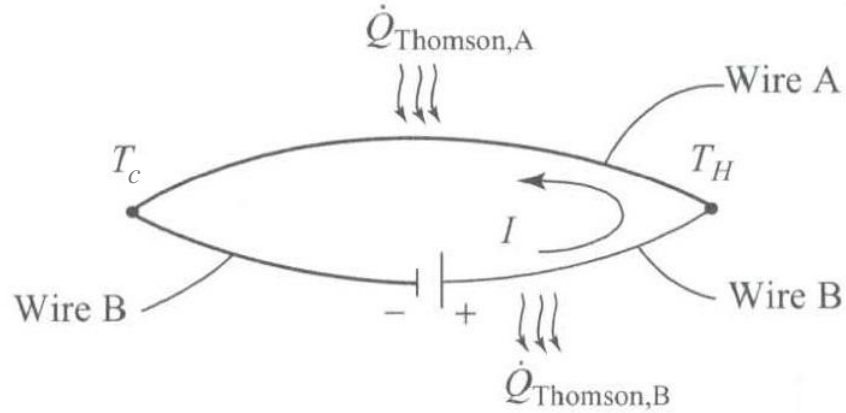


Figure 5. Schematic diagram for the Thomson effect (Lee, 2010).

4. Thomson (Kelvin) relationships

The Thomson/Kelvin relationships relate the Seebeck coefficient to the Peltier coefficient and the Thomson coefficient in a useful manner. Thus, it is demonstrated that all three aforementioned effects are part of the same effect, the thermoelectric effects.

The first Thomson relation is:

$$\pi_{AB} = \alpha_{AB}T \quad (7)$$

And the second Thomson relation is given by:

$$\tau_A - \tau_B = T \frac{dS_{AB}}{dT} \quad (8)$$

Both relationships were found by applying the First and Second Law of Thermodynamics and assuming that thermoelectric processes can be separated into reversible and irreversible processes. This assumption was a concern for the validity of theory until Onsager's principle helped to confirm the Thomson relationship in 1931

(Lee, 2010; Onsager, 1931).

II. RESEARCH OBJECTIVE

The main objective of this work is to analytically describe and to experimentally measure the power production and the influencing factors for an aqueous Copper II Sulfate Pentahydrate electrolyte based thermo-electrochemical cell. This thermogalvanic cell configuration is comprised of two copper electrodes and the aqueous $\text{CuSO}_4 \cdot 5\text{H}_2\text{O}$ electrolyte. When the electrodes are subjected to a temperature gradient and a potential difference is produced, current can be discharged to power external devices. The maximum power production is influenced by many different factors. Three very identifiable factors however, are the concentration of the Copper II Sulfate Pentahydrate electrolyte, the electrode spacing (distance between the two electrode plates), and the electrode surface area.

Since concentration is a major driving force in the power production of a thermocell, the effect of changing concentrations on the power production is researched in this study. Higher concentrations of electrolyte result in more ions available for current flow and higher power production, as expected by the Butler-Volmer model (Quickenden & Mua, 1995). Another reason why the concentration is important stems for the economy sustainability of thermocell design. The electrolyte is one of the major, costly components and depending on the material used, higher concentrations will increase the

price rapidly. This study is particularly focused on the performance of low electrolyte concentration thermogalvanic cells due to the cost advantage for commercial use.

Another goal is to find a relationship between electrode spacing and maximum power production for the $\text{CuSO}_4 \cdot 5\text{H}_2\text{O}$ electrolyte. Depending on the distance between the two copper electrodes ion movement will be faster or slower. Faster ion flow means a higher current flow and thus power production. Depending on the optimal spacing for the $\text{CuSO}_4 \cdot 5\text{H}_2\text{O}$ electrolyte, copper electrode combination, this thermocell could be a viable low grade heat energy source for either small- or large scale applications. Previous studies of different electrolytes have found that a decrease in electrode spacing resulted in an increase in performance (Kang et al., 2012). The present study aims to either confirm or disprove the same behavior for the Copper II Sulfate Pentahydrate electrolyte.

Changing the electrode surface area and its performance impacts were also studied in this thesis. Kang et al. showed that for some thermogalvanic cells power increased when the surface area was increased due to more available reaction sites for the redox reaction (Kang et al., 2012). The Copper II Sulfate Pentahydrate based thermocell is investigated to determine if it shows the same trends. Additionally, the effect of a changing surface area with respect to the efficiency is also examined.

This study investigates the heat transfer (conduction) within the electrolyte of $\text{CuSO}_4 \cdot 5\text{H}_2\text{O}$ thermocells for different electrode separations. The power conversion efficiency equation accounts for the electrode separation since the heat flow will be influenced by the distance between the electrodes. Heat conduction will lower the temperature difference and hence decrease the potential difference across the

two electrodes. Since this is an unfavorable effect for a thermogalvanic cell, electrode spacing should be chosen carefully to avoid excess heat transfer within the electrolyte.

In summary, all research objectives for the present study, including some smaller aims are the following:

- CuSO₄ 5H₂O electrolyte concentration effect on power production
(Experimental)
- Copper plate electrode spacing effect on power production (Experimental)
- Electrode surface area effect on power production (Experimental)
- Heat transfer analysis for CuSO₄ 5H₂O (aq.) electrolyte (Simulation)
- Electrode spacing effect on internal resistance (Experimental)
- Electrode spacing effect on efficiency (Experimental)

III. PERFORMANCE OF THE THERMOCELL

The performance of a thermogalvanic cell is best described in terms of its output potential which can be directly measured. Knowing the output potential and the corresponding current, the power output can be calculated using Ohm's Law.

$$P = \Delta V \cdot I \quad (9)$$

Where P is the power output, ΔV the potential difference, and I the current. Some publications will feature the figure of merit (Z), a non-dimensional ratio used to describe the performance of solid thermoelectric devices (Quickenden & Mua, 1995),

$$Z = \frac{\alpha^2 \sigma}{k} \quad (10)$$

where σ and k are the ionic and thermal conductivity of the electrolyte and α is the Seebeck coefficient. The ionic conductivity however, is not necessarily a constant for all thermocells and thus will not always behave ohmic in nature. The behavior heavily depends on the electrode and electrolyte material. Hence it is advised to avoid using figure of merit, Z, to describe the performance of a thermocell (Quickenden & Vernon, 1986).

The maximum power can be found when looking at the I- ΔV diagram. If the curve is approximately linear, the maximum power is the largest rectangle under the curve, or

$$P_{max} = \left(\frac{\Delta V_{oc}}{2}\right)\left(\frac{I_{sc}}{2}\right) = \frac{\Delta V_{oc}^2}{4R_{int}} \quad (11)$$

where ΔV_{oc} is the open circuit potential, I_{sc} the short circuit current, and R_{int} the internal resistance (Quickenden & Mua, 1995). If the relationship between I and ΔV is not linear, the maximum can still be computed using basic math techniques. If the relationship between I and ΔV is linear however, then the greatest area under the I- ΔV curve (P_{max}) occurs at $\Delta V=0.5V_{oc}$. At this point the internal resistance of the thermocell equals the external resistance ($R_{int}=R_{ext}$) and the above relationship can be expressed as:

$$P_{max} = \frac{\Delta V_{oc}^2}{4R_{ext}} \quad (12)$$

A performance term that is often used to describe a thermogalvanic cell is the power conversion efficiency, η_{pc} . This quantity is defined as (Quickenden & Mua, 1995)

$$\eta_{pc} = \frac{\text{electrical output power}}{\text{thermal power flowing through cell}} = \frac{P_{max}}{\left[kA\left(\frac{\partial T}{\partial x}\right) + \frac{IT\Delta S}{nF}\right]} \quad (13)$$

The thermal power flowing through the cell accounts for the rate for heat transfer due to thermal conduction and the rate of heat transfer through the cell due to reversible heat of the reaction. This last term should only be included if there is a net consumption of the electrolyte (Quickenden & Vernon, 1986). If there is no net consumption then the equation for the power conversion efficiency simplifies to,

$$\eta_{pc} = \frac{P_{max}}{kA\left(\frac{\partial T}{\partial x}\right)} \quad (14)$$

where κ is the thermal conductivity, A the surface area of the electrode, ∂T the temperature gradient between The power conversion efficiency is usually compared to the Carnot efficiency, so that the relative efficiency, η_r , is defined as

$$\eta_r = \frac{\eta_{pc}}{\eta_c} = \frac{\eta_{pc}}{1 - \frac{T_{cold}}{T_{hot}}} \quad (15)$$

IV. THERMOCELL DESIGN CONSIDERATIONS:

A high Seebeck coefficient is a first requirement to high thermocell efficiency.

This equates to a high equilibrium potential difference for a given temperature difference.

Various redox couples have been researched for their Seebeck coefficients and some have

been studied for thermocell applications such as the $\text{Fe}(\text{CN})_6^{4-}/\text{Fe}(\text{CN})_6^{3-}$ redox couple.

Electrode Reaction	$(\partial V/\partial T)$ [mV K ⁻¹]
$\text{Ra} \leftrightarrow \text{Ra}^{2+} + e^-$	0.28
$\text{H}(\text{g}) \leftrightarrow \text{H}^+ + e^-$	1.382
$\text{Fe} \leftrightarrow \text{Fe}^{2+} + 2e^-$	0.932
$\text{Cu} + \text{I}^- \leftrightarrow \text{CuI} + e^-$	0.671
$\text{Ag} + \text{Br}^- \leftrightarrow \text{AgBr} + e^-$	0.363
$\text{Ag} + \text{Cl}^- \leftrightarrow \text{AgCl} + e^-$	0.213
$\text{Cu} \leftrightarrow \text{Cu}^{2+} + 2e^-$	0.879
$\text{U}^{3+} \leftrightarrow \text{U}^{4+} + e^-$	1.02
$\text{Fe}^{2+} \leftrightarrow \text{Fe}^{3+} + e^-$	0.771
$\text{Tl} + \text{OH}^- \leftrightarrow \text{Tl}(\text{OH}) + e^-$	0.003
$\text{Pb}^{2+} + 2\text{H}_2\text{O} \leftrightarrow \text{PbO}_2 + 4\text{H}^+ + 2e^-$	0.633
$\text{Zn} + 4\text{CN}^- \leftrightarrow \text{Zn}(\text{CN})_4^{2-} + 2e^-$	1.19
$\text{Hg} + 4\text{CN}^- \leftrightarrow \text{Hg}(\text{CN})_4^{2-} + 2e^-$	1.65
$\text{Fe}^{3+} \leftrightarrow \text{Fe}^{2+} + e^-$	0.75
$\text{Fe}(\text{CN})_6^{3-} \leftrightarrow \text{Fe}(\text{CN})_6^{4-} + e^-$	1.5
$\text{Np}^{3+} \leftrightarrow \text{Np}^{4+} + e^-$	2 - 2.25
$\text{Pu}^{4+} \leftrightarrow \text{Pu}^{3+} + e^-$	2 - 2.25
$\text{Fe}(\text{CN})_6^{4-} \leftrightarrow \text{Fe}(\text{CN})_6^{3-} + e^-$	7.4

Figure 6. Seebeck coefficient comparison for different redox couples (deBethune, Licht, & Swendeman, 1959).

The ratio of the charge carrier flux to the thermal flux should be kept high to ensure a strong power delivery. This can be expressed through the ratio of the electrical to thermal conductivity σ/k . Reducing the thermal conductivity by adding thermal

barriers to the electrolyte can improve the performance of thermocell. A thermal barrier material such as powdered silica will help to increase the efficiency and power output (Cadoff, 1960).

A. Electrode Spacing

A decrease in electrode separation leads to an increase in output power due to the mass transport overpotentials for most electrolytes. However, more thermal energy is required to keep a constant temperature difference because of increased inter-electrode heat transport (Kang et al., 2012).

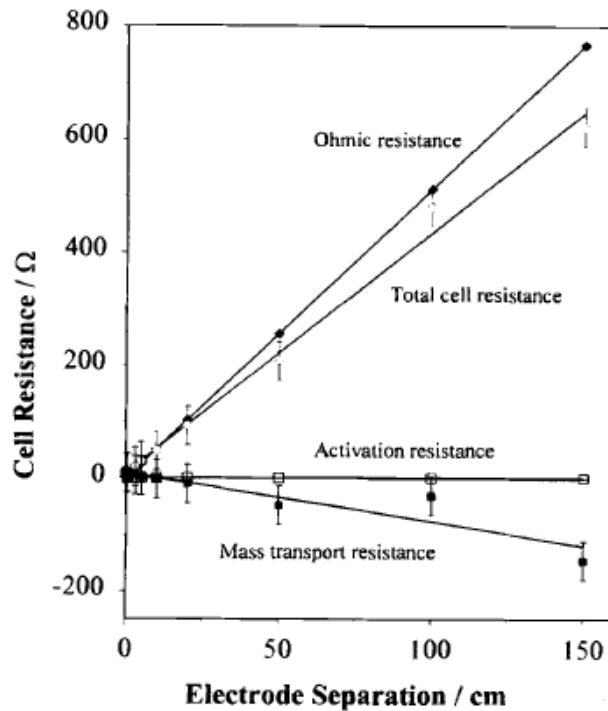


Figure 7. Effect of electrode separation on thermocell resistance (Mua & Quickenden, 1996).

The graph shows that the Ohmic resistance has the greatest influence on the total resistance whereas the mass transport resistance positively contributes to the total cell resistance. Thus it would be desirable to keep the Ohmic resistance at a minimum to reduce the overall resistance of the thermocell. An increase in electrode separation linearly increases the internal resistance. Other literature suggests that cleaning the electrode surface can decrease the internal resistance (Mua & Quickenden, 1996; Randles & Somerton, 1952).

Power conversion efficiency and maximum power density are both dependent on electrode separation. However, they have inverse relationships with electrode spacing when compared to each other as the following graph shows.

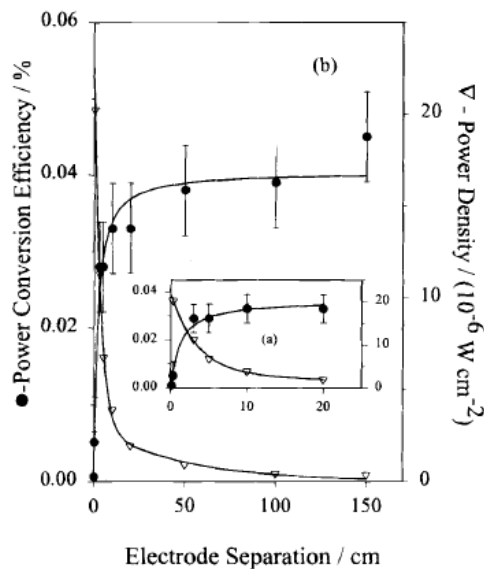


Figure 8. Effect of electrode separation on Power conversion efficiency (Mua & Quickenden, 1996).

The small graph inside the figure is merely a magnification for the electrode separation values ranging from $d=0$ to 25 cm. It has been demonstrated that a high power density does not correlate to high power conversion efficiency. A 0.09 % Carnot

efficiency is calculated with the maximum power density of $2200 \mu\text{Wcm}^{-2}$ as reported by Ikeshoji et al.(Ikeshoji & Gonçalves, 1993). On the other hand, a lower power density of $3.7 \mu\text{Wcm}^{-2}$ correspond to a Carnot efficiency of about 0.50 % as it was reported by Quickenden et al.(Quickenden & Mua, 1995).

B. Electrode Size Effect

Optimal electrode sizing will decrease the internal resistance of the cell. By increasing the surface area of the electrodes more reaction sites become available during a reaction and the output current is increased. For example, for a SWNT electrode the sheet electrode area was increased from 0.25 to 1.0 cm^2 and the current increased from 0.38 to 0.72 mA . A linear relationship between the maximum output power and the electrode size was detected by one study (Kang et al., 2012).

Increasing the size asymmetrically may help the power generation for a thermocell. When the cold electrode was 4 times the size of the hot electrode, an increase in power of around 10 % was witnessed. Any other configurations did not yield positive results. The cold electrode has smaller redox rate per unit surface area and thus it is important to match the redox rates for both side so that a steady state current can flow (Kang et al., 2012).

C. Effect of Electrolyte Concentration

Increasing the electrolyte concentration of the redox couple for a thermocell improves the power output and decreases the cell resistance. This relationship is expressed in the Bulter-Volmer equation. (Quickenden & Mua, 1995). This effect is

caused by an increased number of redox ions that can interact with the electrodes and also an increase in electrical conductivity for the electrolyte (Kang et al., 2012).

Thus a higher power output is linearly proportional to a higher electrolyte concentration. Some studies have suggested that a higher electrolyte concentration can slow down ion movements and built up products at reaction sites (Kang et al., 2012). Other studies have also suggested that there is an optimal value for the electrolyte concentration after which an increase will not yield better performance. Gunawan et al. confirm the previous theory and just added that the internal resistance would most likely be a factor for the phenomenon (Gunawan et al., 2013).

1. Electrolyte Concentration versus temperature difference effect on the potential difference:

Thermocell electrolytes show very different performance characteristics depending on the electrolyte concentration. First, with most concentration amounts it is noticed that once the ΔT goes beyond a certain threshold the performance will go down drastically. Similarly, when keeping the concentration constant, certain temperature differences can be found that exhibit better performance than most other ΔT values. This might be attributed to the fact that water in the electrolyte may have vaporized and so allowed solid phase electron transfer (Manda et al., 2013).

At a different concentration a linear increase of ΔV was noticed until a threshold was reached and the performance suffered. This linear increase in performance could be explained through the solid phase redox reaction for a ΔT and then the electrolyte degraded after a certain temperature difference was reached (Manda et al., 2013).

However, this linear increase is not observed for all electrolyte concentrations. In this particular study, the concentration was increased by 40 times and a decreased of ΔV was seen when ΔT was increased. A cause might be the instability of the electrolyte (Manda et al., 2013).

The short circuit current exhibits similar behavior to electrolyte concentration and temperature difference as described above for the potential difference (Manda et al., 2013).

2. Electrolyte Concentration vs temperature difference effect on the max power output and power density:

The power density remained constant from $\Delta T = 30\text{ }^{\circ}\text{C}$ to $70\text{ }^{\circ}\text{C}$ and decrease rapidly with increase in ΔT from $80\text{ }^{\circ}\text{C}$ to $120\text{ }^{\circ}\text{C}$. The maximum power output increased from $\Delta T = 30\text{ }^{\circ}\text{C}$ to $70\text{ }^{\circ}\text{C}$ and then decreased dramatically for temperature differences above $80\text{ }^{\circ}\text{C}$ (Campbell, 1999). Thus there is also a threshold for the power density in relation to the electrolyte concentration.

D. Cell Orientation Effect on Performance

The way a thermocell is physically build has an effect on the performance. Three different structure were analyzed: 1) horizontal electrodes with the hot side on top and the cold side on the bottom, 2) same electrode arrangement but the cold side on top and hot on the bottom, and 3) vertically parallel electrodes (here the temperature orientation does not matter).

The orientation influences the electron mass transport. When correctly aligned, natural convection will aid the electron transport through the electrolyte and result in a higher power output. With a bad orientation a natural convection effect will not influence the mass transport, as it happens with case 1) where the hot electrode side is on top of the cell arrangement. When physical built-up 2 or 3 are used the power output of the thermocell will increase by up to 140 % to cell 1 (Kang et al., 2012).

The convective mixing (various types working together) affects the time dependence of internal resistance and aids the ion transport (Kang et al., 2012).

Cell potential and output current are determining factors in a thermocell for the capability to generate power. The cell potential is proportional to the temperature difference between the two electrodes and the thermoelectric coefficient of the redox couple. For a set temperature difference the internal resistance of a cell can negatively affect the output current.

E. Internal resistance as a factor for cell performance

Internal resistance of the electrolyte has an impact on the cell performance. Three factors contribute to the internal resistance of the cell. Ohmic, mass transport, and activation resistance all add to the internal resistance of the cell. In previous studies these three effects have been measured and graphically illustrated (Mua & Quickenden, 1996).

Many factors contribute to the total internal resistance and not all can be eliminated or minimized such as the internal resistance of wiring. Other internal resistances in a thermocell are attributed to the electrolyte, electrodes, and the electrolyte and electrode interface. As the electrolyte concentration increases the internal resistance

of a thermogalvanic cell decreases (Tester, 1992). This phenomenon can be explained by the increase of electrolyte conductivity due an increase in ion density at higher concentrations. Thus the ions can move more easily through the electrolyte. The following graph illustrates this behavior but also shows, as in other studies (Gunawan et al., 2014), that there is an upper bound at which increasing the electrolyte concentration will not yield a better performance.

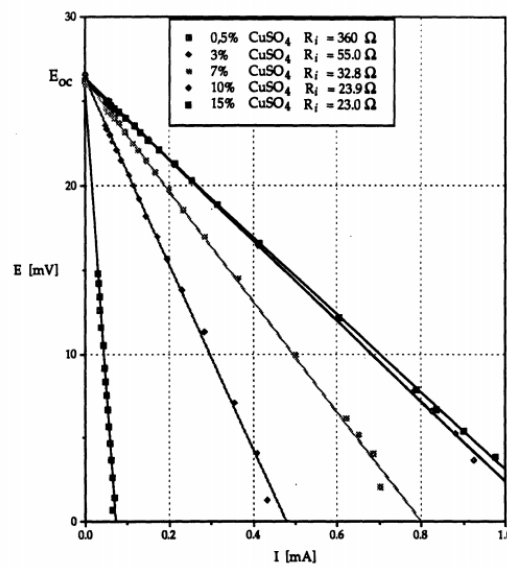


Figure 9. Concentration Dependence on R_{int} (Tester, 1992).

Internal resistance can also be dependent on the operating time. As it was shown for the electrolyte CuSO_4 the internal resistance of the electrolyte greatly increased after a day of operating the thermocell (Tester, 1992).

V. EXPERIMENTAL SETUP AND PROCEDURE

For experimental testing of a thermo-electrochemical cell different setups were used to explore different properties and to obtain accurate experimental values. Different sizes and heating methods were used in order to improve results.

The first testing equipment provided by PINE Instruments© is an electrochemical testing device. A 6 inch long diameter tube can be filled with the electrolyte. At each end a mounting is fitted to hold the copper electrode plate. The mounting was closed using acrylic glass and silicone rubber to immerse the cold electrode side into a water bath. The warm electrode was closed in similar fashion to insulate it with fiberglass wool. Openings of the testing equipment were closed with stoppers to avoid vaporization of the electrolyte escaping to the ambience. The warm electrode was heated using a hot plate and a hot air gas supply line from a fuel cell testing supply line. The hot air supply line provided humidified air to the hot electrode via a nozzle. Temperature of the hot air was controlled with a computer using a thermocouple to measure the temperature right before exiting the nozzle. Two additional thermocouples were applied to each electrode to measure the temperature difference. Due to the manual control of temperature gradient small deviations from the desired value were expected (around $\pm 1^{\circ}\text{C}$). Constant monitoring of the thermocouple output was used to minimize the error.

The copper electrode plates were connected to an Arbin Instruments© testing and data logging system. This system will automatically record current and potential

difference. The accuracy is within 0.02% for any low-power application. In addition, the Arbin Instruments© system can charge or discharge the cell at a controlled rate to measure the power production of the thermocell. Testing schedules can be setup via a computer control panel.

For open circuit voltage tests the hot air stream was set to 90 °C and the nozzle placed three centimeters away from the warm electrode plate. Additionally, a hot plate set to 65 °C heats an Aluminum plate at the bottom of the electrode housing. The cold electrode side housing is filled with cold iced water (temperature at around 15 °C) and depending on the length of the test more cold water or ice cubes are added to keep the temperature nearly constant. Tests were usually run for around an hour to establish a constant temperature difference and have steady ion flow in the thermogalvanic cell.

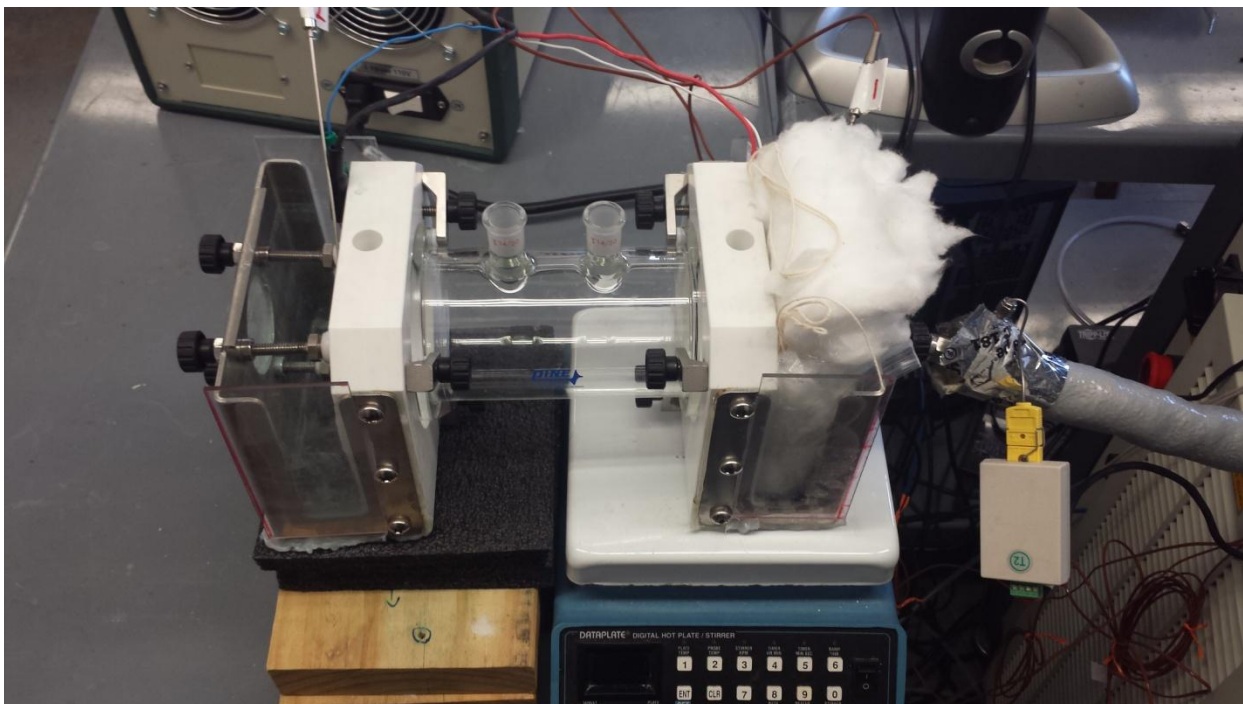


Figure 10. Full electrochemical test cell equipment. Warm electrode is on hot plate and connected to hot air supply stream, Cold electrode can be submersed in a cold water bath.

Another testing setup was used to measure the properties of a thermogalvanic cell. The previous system was modified to simulate different electrode spacings and electrolyte volumes. Thus, the glass cell was removed and a two inch diameter borosilicate glass tube from ABR Imagery© was used. Custom Glassblowing of Louisville, Inc. cut a two and a three inch piece to use as the electrolyte container. As previously mentioned the hot electrode was heated with moist air (varying from 35 °C to 85 °C) and the cold side was subjected to an iced water bath to keep the temperature difference constant. Additionally, the hot plate was set to around 50 °C to aid the heating of the warm electrode side. Thermocouples at each end measured the temperature of the electrodes. The copper plate electrodes were connected to the same Arbin Instruments© testing and data logging equipment to measure current and potential difference.

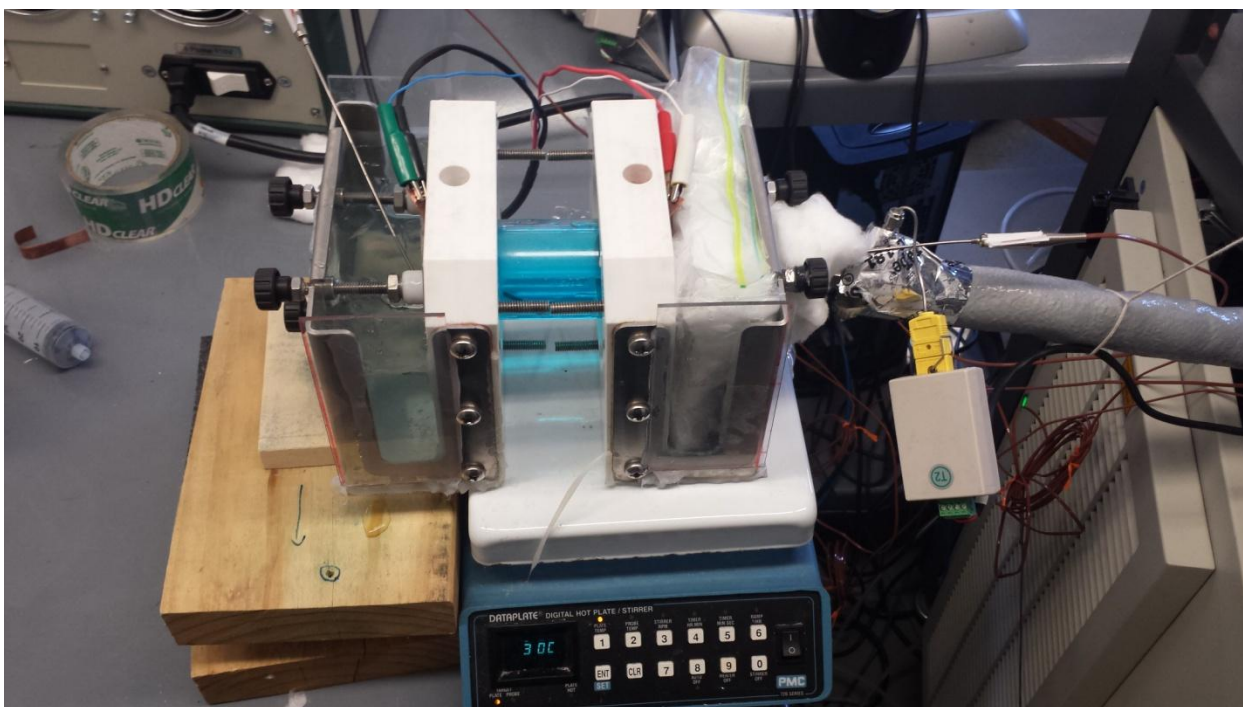


Figure 11. Modified electrochemical test cell equipment with a three inch borosilicate glass tube. Cold electrode is in iced water bath and warm electrode is on hot plate and supplied with hot moist air.

A beaker – salt bridge testing system was set up using small beakers (maximum volume at 30 milliliters). The salt bridge was established using Kimtech© filter paper. The warm electrode beaker was set on a hot plate (temperature set to 225 °C) while the cold electrode beaker was left at ambient temperature (around 22 °C). Strips of copper were placed into each beaker along with a thermocouple to measure the temperature of each electrode. Tests were conducted from 45 min to 90 min for a constant temperature difference and steady ion flow across the salt bridge. Arbin Instruments© data logger and measurement system was used to record the experimental data.

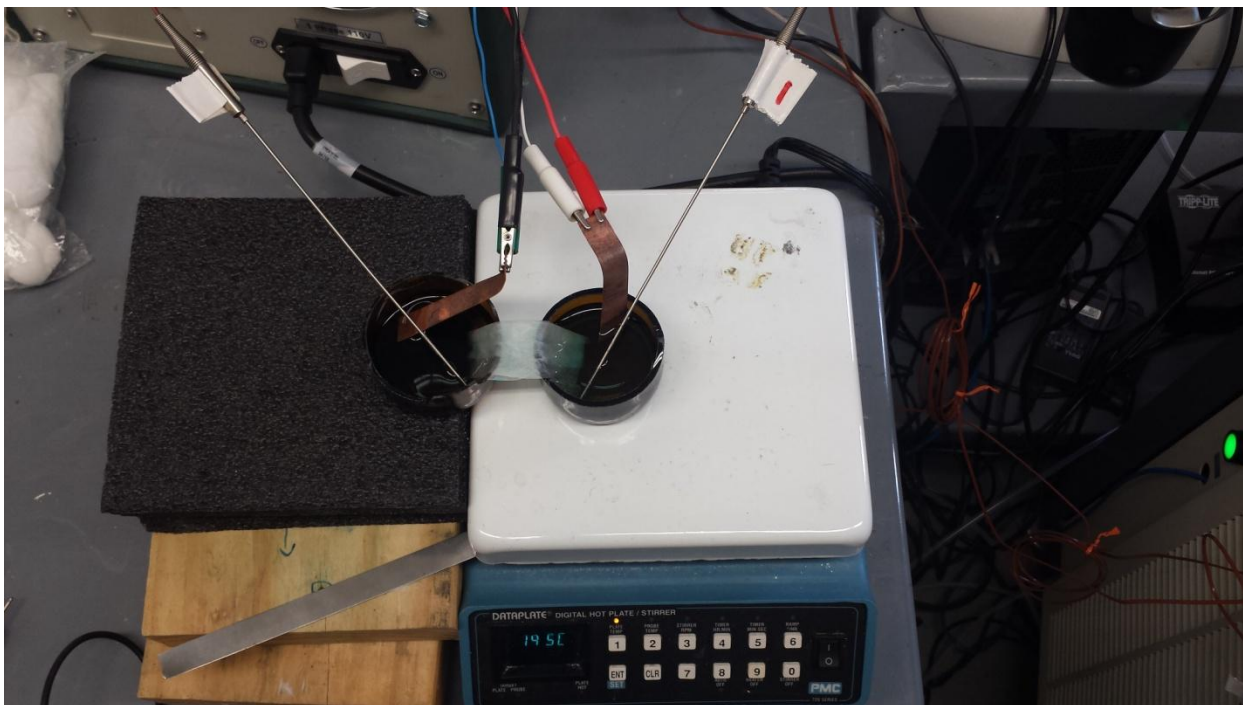


Figure 12. Small volume beaker setup with filter paper salt bridge. Warm electrode is on hot plate and cold electrode is at room temperature.

A. Electrode pretreatment

All copper electrodes were pretreated before each test cycle. First, the electrode plates were sanded down to remove all residual electrolyte built up and impurities from previous tests. Then they were rinsed with water and dried with Kimtech wipes to removed copper sanding dust. Additional clearing with ethanol, rinsing and drying with Kimtech wipes concluded the cleaning.

B. Electrolyte preparation

The electrolyte used for the experiments was Copper II Sulfate Pentahydrate, $\text{CuSO}_4 \cdot 5\text{H}_2\text{O}$, purchased from SigmaAldrich Corporation. For preparation of the aqueous

electrolyte deionized water was used. The granulate $\text{CuSO}_4 \cdot 5\text{H}_2\text{O}$ was combined with the deionized water in a beaker and the solution was mixed using a stirrer. After stirring the electrolyte was immediately transferred to the testing equipment to avoid any contamination.

C. Thermocell testing cycles

1. Open circuit voltage testing

For the open circuit voltage testing the thermocell was connected to Arbin Instruments© data logging system. Neither an external current nor potential difference was applied to the thermocell. Only the potential difference imposed by the Seebeck effect was measured. The temperature gradient was recorded with the voltage difference so that the Seebeck coefficient can be determined. The following two graphs give an example of the resultant test data. Figure 13 shows the potential difference and Figure 14 is the analogous temperature difference recorded by the thermocouples.

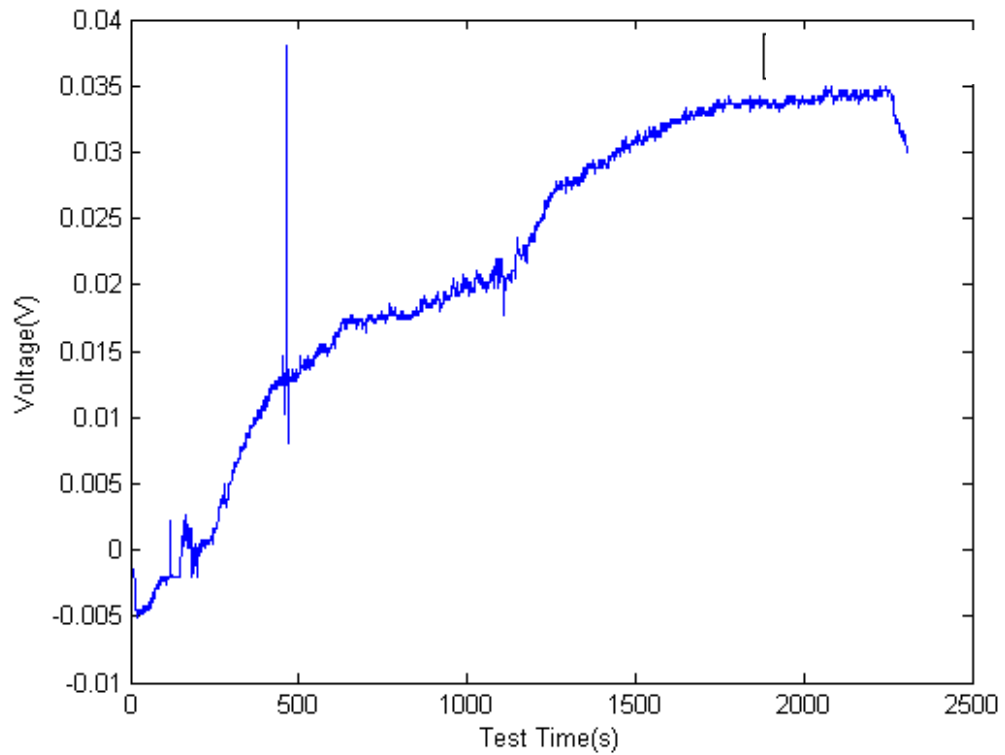


Figure 13. Open Circuit Voltage Test from 2/20/2015 with 0.01M $\text{CuSO}_4 \cdot 5\text{H}_2\text{O}$ concentration and 6 inch electrode separation.

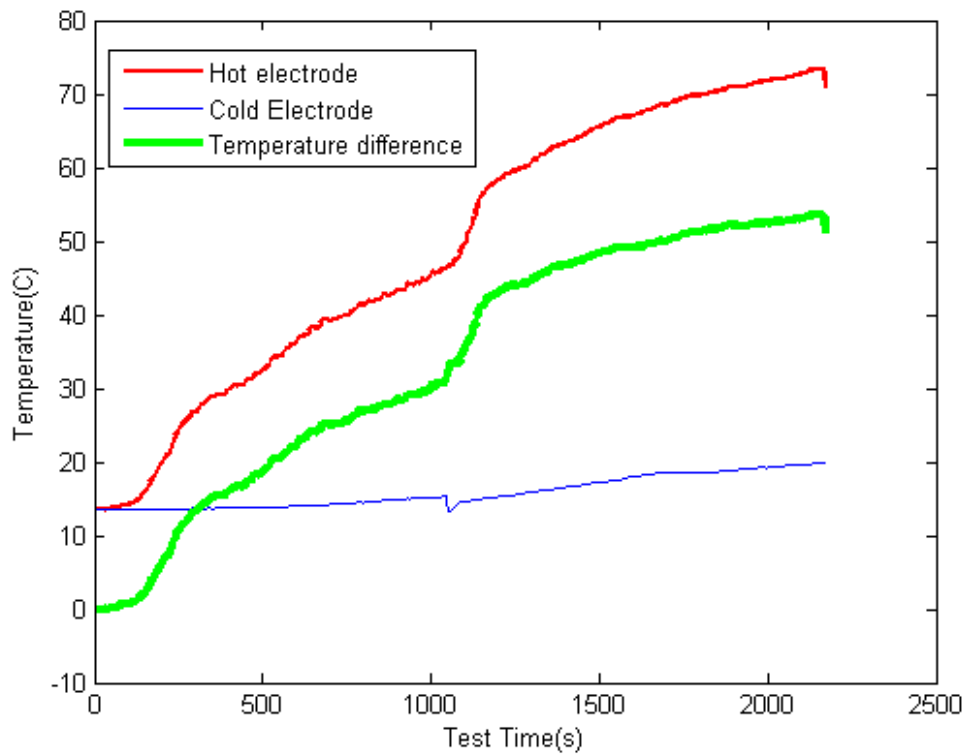


Figure 14. Temperature Difference for Test 02/20/2015 (Fig13.).

2. Discharge testing

The power production capabilities of the thermocell were tested using the Arbin Instruments© testing system. A specific test cycle was set up which was used for every configuration and variation of the thermocell. An initial rest period of five minutes was used to record the open circuit voltage and to establish the desired temperature difference. Next, a discharge current of 0.1 mA was applied for four minutes. This discharge current was increased by 0.1 mA up to 1 mA with each cycle running for four minutes. Lastly, four additional cycles discharged current (5 mA, 10 mA, 15 mA, and 20 mA; four minutes each.) The logged data was converted into an Excel Spreadsheet with an Arbin Instruments© provided Add-In.

The following figures show examples for a discharge testing plot. Figure 15 shows a test cycle discharging current from $I = -0.1$ mA to $I = -0.5$ mA and Figure 16 shows a testing cycle over the previously described range. The temperature difference was monitored throughout the whole test cycle to ensure good results.

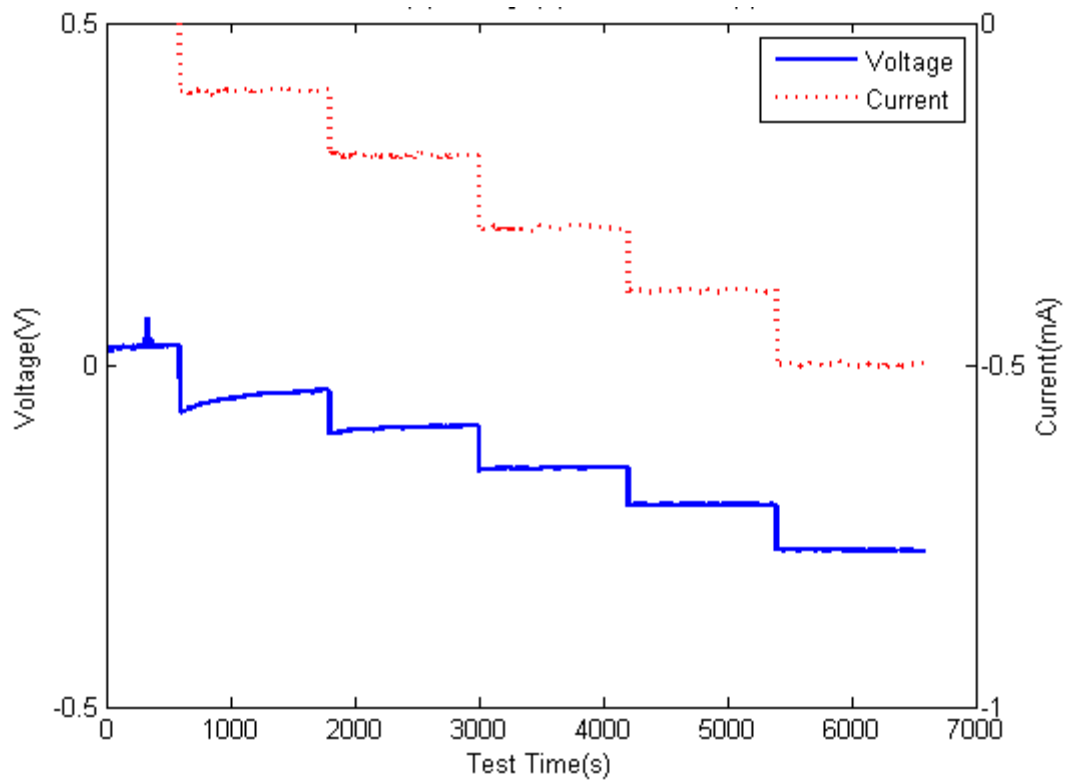


Figure 15. Test from 2/26/15 with 0.01M $\text{CuSO}_4 \cdot 5\text{H}_2\text{O}$ concentration, 6 inch electrode separation and current discharge steps ranging from 0.1 mA to 0.5 mA (step increase of 0.1 mA) at $\Delta T = 30^\circ\text{C}$.

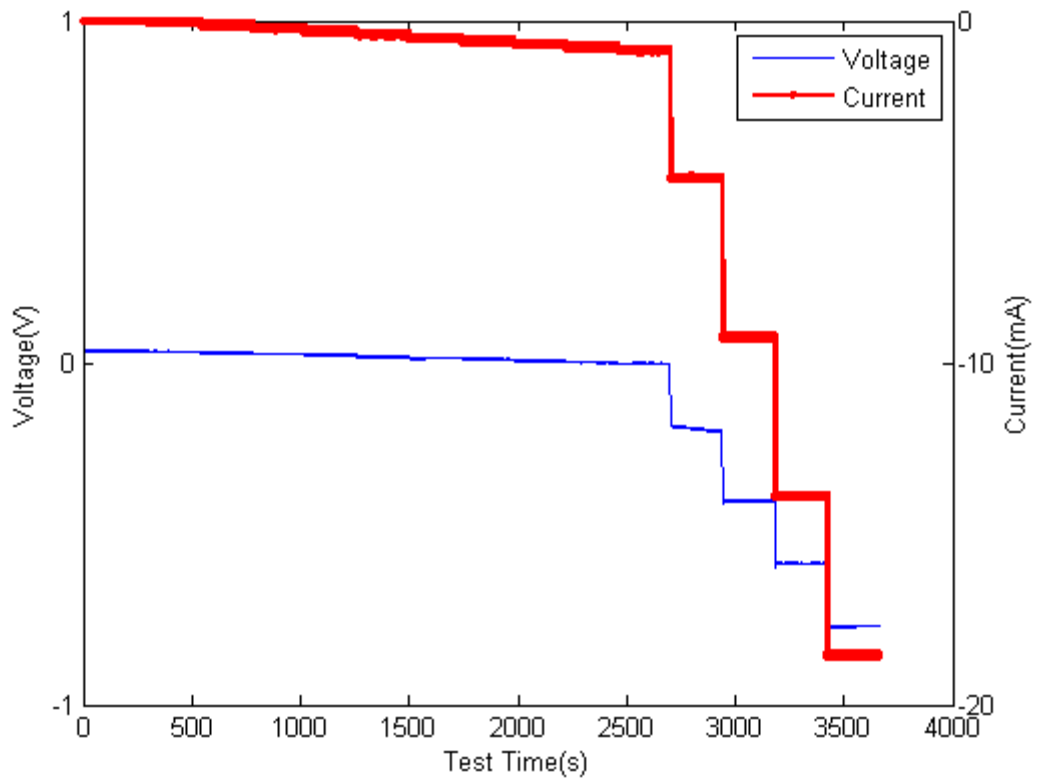


Figure 16. Test from 4/25/2015 with 0.3M $\text{CuSO}_4 \cdot 5\text{H}_2\text{O}$ concentration and 6 inch electrode separation, discharging steps from $I = -0.1 \text{ mA}$ to $I = -20 \text{ mA}$ at $\Delta T = 50 \text{ }^\circ\text{C}$.

VI. RESULTS AND DISCUSSION

Since the performance of the thermogalvanic cell is heavily dependent on the properties of the electrolyte, various tests were conducted evaluating different parameters to quantify its performance. The Seebeck coefficient is used to compare different parameters important for an efficient thermo-electrochemical cell.

1. Seebeck coefficient dependence on concentration

The following figure shows the Seebeck coefficients for different concentrations of $\text{CuSO}_4 \cdot 5\text{H}_2\text{O}$ (Copper (II) Sulfate Pentahydrate) electrolyte. All Seebeck coefficients are measured with the same thermocell setup (6 inch electrode spacing) and average over the temperature gradients $\Delta T = 10\text{-}50\text{ }^\circ\text{C}$.

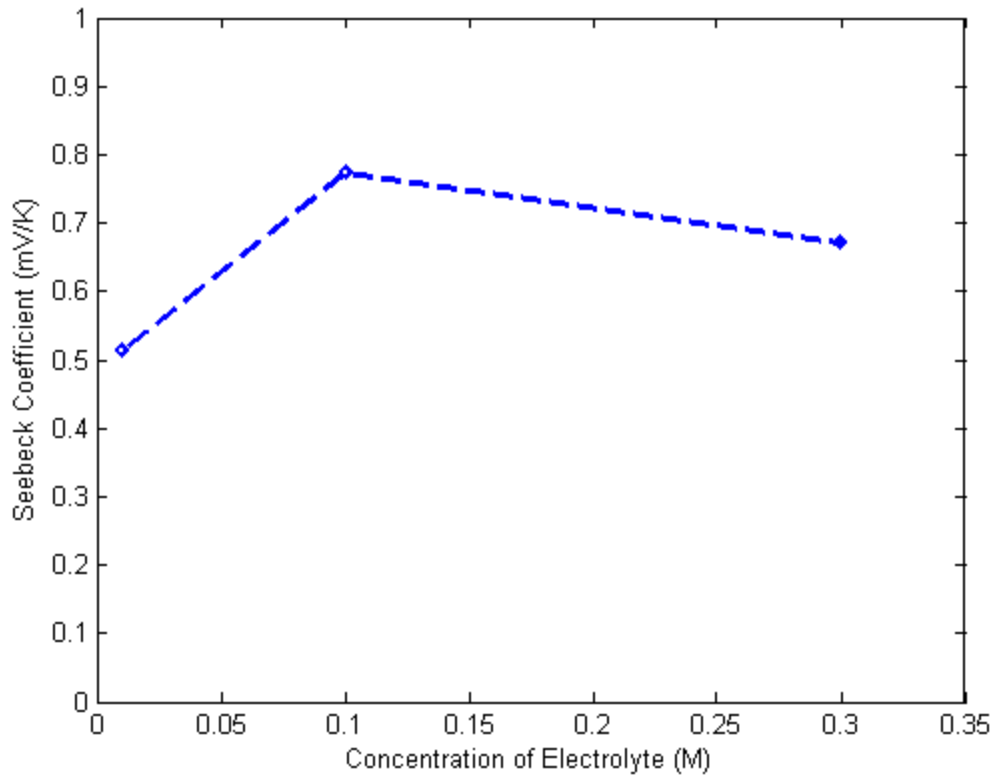


Figure 17. Experimental results of Seebeck coefficient dependence on concentration testing for Copper (II) Sulfate Pentahydrate with copper electrodes.

From the experimental results it is noticed that for a given electrolyte there is an optimal concentration at which the Seebeck coefficient will be highest. This optimal value will not be the same for all electrolytes but has to be experimentally determined for each one but also heavily depends on the individual thermocell. For this Copper (II) Sulfate Pentahydrate thermocell setup the optimal value is rather low at 0.1M. The highest Seebeck coefficient measured, however, was close to the maximum value observed in other studies (Gunawan et al., 2013). A low optimal concentration would make $\text{CuSO}_4 \cdot 5\text{H}_2\text{O}$ a desirable electrolyte material since for larger size thermogalvanic cells the cost would be kept relatively low.

2. Seebeck coefficient dependence on electrode area

The Seebeck coefficient dependence on electrode surface area was also investigated in this study. All tests were run with a concentration of 0.3M $\text{CuSO}_4 \cdot 5\text{H}_2\text{O}$ and the Seebeck coefficient was average for all tests since the discharge behavior showed linearity. As seen in the subsequent graph the Seebeck coefficient is very stable when the surface area is changed. The increase is very miniscule and thus it is concluded that the effect of changing the electrode surface area on the Seebeck coefficient is negligible.

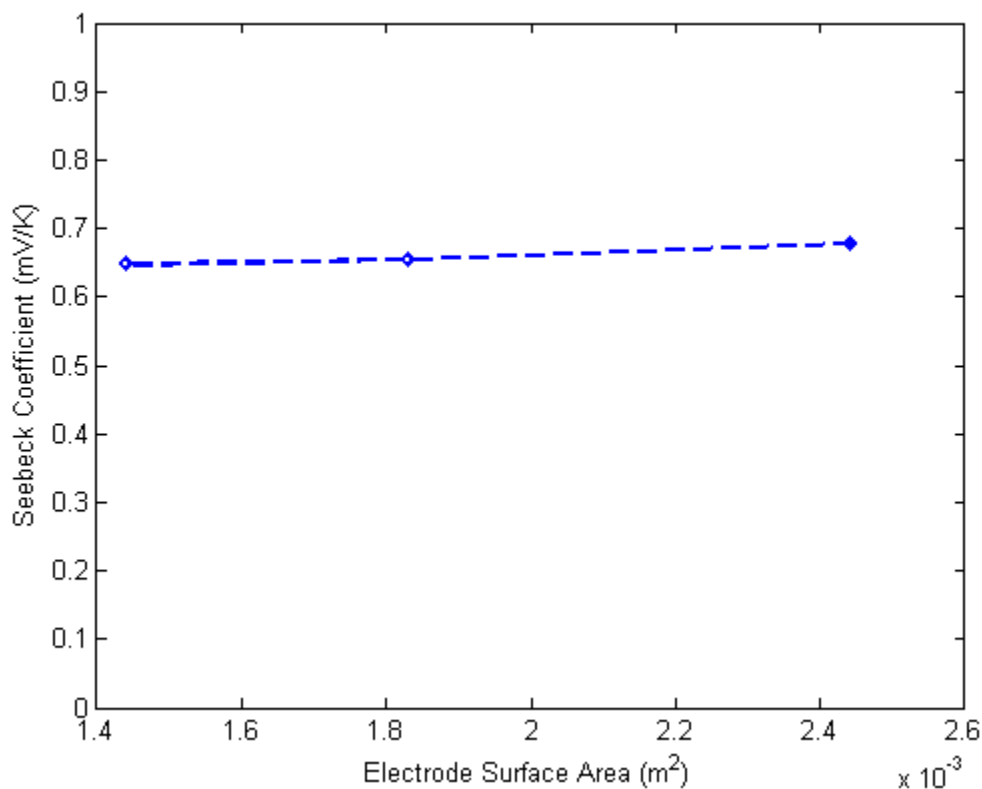


Figure 18. Experimental results of Seebeck coefficient dependence on electrode surface area testing for Copper (II) Sulfate Pentahydrate with copper electrodes.

A. Power production testing/ discharge capabilities of a thermocell

The power production of each thermogalvanic cell configuration was tested for comparison of different factors and systems. The following analysis shows the interrelationship between heat gradient and electrolyte concentration, both affecting the performance of the thermocell. The first three experiments are all conducted with an electrode separation of $d= 6$ inches (0.1524 m), an electrode surface area of $A= 0.00244$ m² and an electrolyte volume of 0.5 L.

1. Characterization of 0.01M Copper II Sulfate Pentahydrate based thermocell

For 0.01M concentration of Copper II Sulfate Pentahydrate a relatively poor performance is expected based on previous literature results (Gunawan et al., 2013). It is valuable, however, to explore the performance of low concentration based thermocell due to the economical value. The I-V curve (Figure 19) shows negative values for the current since current is discharged. Voltage measurements show mostly a negative potential during each discharge cycle, although this is not necessarily true for all configurations.

The maximum open circuit voltage was measured at $V_{oc}= 0.0262$ V but depending on the temperature gradient it ranged from $V_{oc}=0.0108$ V to 0.0262 V. The maximum Seebeck coefficient measured was $\alpha= 1.08$ mV/K at $\Delta T=10$ °C. This values is one magnitude higher than all others and based on previous literature one would expect the same Seebeck coefficient for all temperature gradients (Gunawan et al., 2013). This behavior is also observed in the current study exhibited by the linear nature of the I-V

discharge graph. Leaving out this anomaly the Seebeck coefficient is relatively constant at around $\alpha = 0.5120$ mV/K for 0.01M CuSO₄. Hence, an increase of the temperature gradient between the electrodes will not result in a better Seebeck coefficient for this redox couple.

Table 1

Characterization of 0.01M Copper II Sulfate Pentahydrate based thermocell

ΔT [°C]	E_{oc} [V]	α [mV/K]	I_{sc} [mA]	J_{sc} [mA/m ²]	P_{max} [μ W]	P_{max}/A [mW/m ²]	Power conversion efficiency	Relative efficiency
10	0.0108	1.0825	0.0135	5.5322	0.0365	0.0150	0.000037	0.000129
20	0.0113	0.5652	0.0154	6.2909	0.0434	0.0178	0.000021	0.000043
30	0.0130	0.4327	0.0185	7.5742	0.0600	0.0246	0.000019	0.000032
40	0.0158	0.5250	0.0240	9.8105	0.0944	0.0386	0.000022	0.000034
50	0.0262	0.5244	0.0428	17.5454	0.2807	0.1150	0.000053	0.000074

The current density was pretty stable for temperature differences $\Delta T=10-30$ °C but maximum at $\Delta T= 50$ °C to $J_{sc}= 17.5454$ mA/m². Here the maximum power output was recorded at $P_{max}/A= 0.1150$ mW/m². The power conversion efficiency, however, was very comparable for temperature differences $\Delta T= 20$ °C, $\Delta T= 30$ °C, and 40 °C, with the latter being slightly higher at $\eta_{pc}= 0.000022$ %. Hence, the relative efficiency (to Carnot efficiency) was at $\eta_r= 0.000043$ % for $\Delta T= 20$ °C compared to $\eta_r= 0.000034$ % at $\Delta T= 40$ °C.

The discharge curves (Figure 19) for 0.01M CuSO_4 are linear and thus the assumption that R_{int} equals R_{ext} is valid. It can be noticed that for $\Delta T= 10\text{-}20\text{ }^\circ\text{C}$ the data points for the $I= -15\text{ mA}$ discharge cycle are missing. This is due to the fact that the Arbin Instruments© testing system is not able to measure a potential higher than $V= 10\text{ V}$ and thus data could not be recorded.

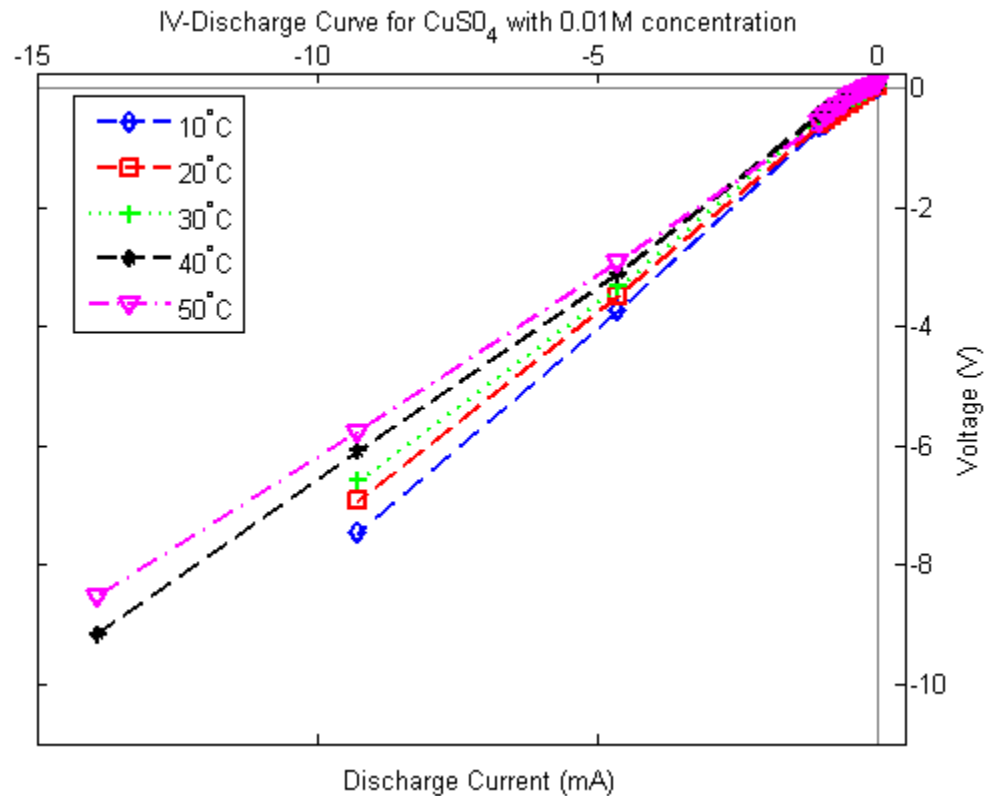


Figure 19. IV-Discharge Curve for 0.01M $\text{CuSO}_4 \cdot 5\text{H}_2\text{O}$ concentration and electrode separation of 6 in. for varying ΔT across the electrodes

2. Characterization of 0.1M Copper II Sulfate Pentahydrate based thermocell

The performance of the 0.1M Copper II Sulfate Pentahydrate cell is expected to be better than the previous 0.01M $\text{CuSO}_4 \cdot 5\text{H}_2\text{O}$ thermogalvanic cell (Gunawan et al., 2013).

Electrode spacing, electrolyte volume, and electrode area were kept identical to the 0.01M CuSO₄ 5H₂O test cycle for accurate comparison.

The Seebeck coefficient for this test cycle was again very constant and averages around $\alpha = 0.7726$ mV/K for 0.1M Copper II Sulfate Pentahydrate with a small margin of error for inaccurate temperature gradients at the time of measurement. Again, this assumption can be made because of the linearity of the I-V discharge curve (Figure 20). Open circuit voltage was at a maximum at $V_{oc} = 0.0373$ V for $\Delta T = 50$ °C and ranged from $V_{oc} = 0.0084 - 0.0373$ V over the complete test range ($\Delta T = 10-50$ °C). The Seebeck coefficient and the open circuit voltage are higher than in the 0.01M CuSO₄ 5H₂O test case, as expected.

Table 2

Characterization of 0.1M Copper II Sulfate Pentahydrate based thermocell

ΔT [°C]	E_{oc} [V]	α [mV/K]	I_{sc} [mA]	J_{sc} [mA/m ²]	P_{max} [mW]	P_{max}/A [mW/m ²]	Power conversion efficiency	Relative efficiency
10	0.0084	0.8362	0.0634	25.9622	0.00013	0.0543	0.00013	0.00047
20	0.0170	0.8491	0.1336	54.7258	0.00057	0.2323	0.00028	0.00056
30	0.0228	0.7610	0.2047	83.8613	0.00117	0.4787	0.00038	0.00062
40	0.0268	0.6708	0.2644	108.2904	0.00177	0.7265	0.00042	0.00063
50	0.0373	0.7460	0.3940	161.3920	0.00367	1.5050	0.00069	0.00096

The current density increases steadily for each test cycle with the maximum value of $J_{sc} = 161.3920$ mA/m² at $\Delta T = 50$ °C. Power output at this temperature gradient is

limited at $P_{\max} = 0.00367 \text{ mW}$. The corresponding power density comes to $P_{\max}/A = 1.5050 \text{ mW/m}^2$ which is fourteen times the maximum power density recorded for the 0.01M test cycle. The power conversion efficiency $\eta_{pc} = 0.00069 \%$ and relative efficiency $\eta_r = 0.00096 \%$ are also significantly improved by an increased in electrolyte concentration.

It is noteworthy that for temperature differences $\Delta T = 30 \text{ }^\circ\text{C}$ and $\Delta T = 40 \text{ }^\circ\text{C}$ the power conversion efficiencies are very similar ($\eta_{pc} = 0.00038 \%$ and $\eta_{pc} = 0.00042 \%$, respectively), again resulting in a higher relative efficiency for the $\Delta T = 30 \text{ }^\circ\text{C}$ cycle compared to the $\Delta T = 40 \text{ }^\circ\text{C}$ ($\eta_r = 0.00062 \%$ and $\eta_r = 0.00063 \%$, respectively.) Hence, an increase in temperature gradient for a 0.1M $\text{CuSO}_4 \cdot 5\text{H}_2\text{O}$ from $\Delta T = 30 \text{ }^\circ\text{C}$ to $40 \text{ }^\circ\text{C}$ would not lead to an improvement in performance.

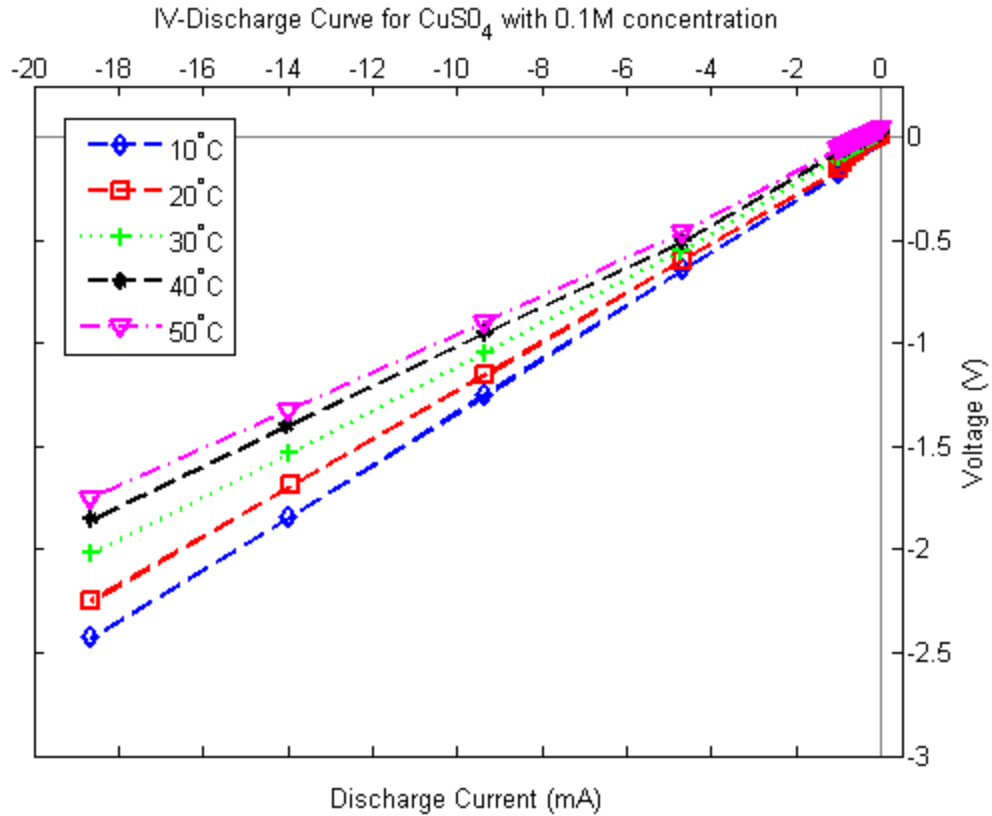


Figure 20. IV-Discharge Curve for 0.1M $\text{CuSO}_4 \cdot 5\text{H}_2\text{O}$ concentration and electrode separation of 6 in. for varying ΔT across the electrodes

3. Characterization of 0.3M Copper II Sulfate Pentahydrate based thermocell

For a 0.3M Copper II Sulfate Pentahydrate based thermogalvanic cell performance improvements are expected compared to the previous two cells (0.01M and 0.1M $\text{CuSO}_4 \cdot 5\text{H}_2\text{O}$). Test cycles and conditions were again kept the same to accurately compare the different thermogalvanic cell setups.

Open circuit voltage for the 0.3M Copper II Sulfate Pentahydrate based thermocell peaked at $V_{oc} = 0.0351 \text{ V}$ at $\Delta T = 50 \text{ }^\circ\text{C}$. Overall, the open circuit voltage ranged from $V_{oc} = 0.0084 \text{ V}$ to 0.0351 V for all temperature gradients. The maximum Seebeck coefficient was recorded at $\Delta T = 10 \text{ }^\circ\text{C}$ as $\alpha = 0.8362 \text{ mV/K}$. Since the I-V

discharge curve is linear the Seebeck coefficient should be constant throughout. Thus averaging the Seebeck coefficient over all temperature differences and accounting for small errors during testing, the Seebeck coefficient is estimated at $\alpha = 0.6706$ mV/K.

Table 3

Characterization of 0.3M Copper II Sulfate Pentahydrate based thermocell

ΔT [°C]	E_{oc} [V]	α [mV/K]	I_{sc} [mA]	J_{sc} [mA/m ²]	P_{max} [mW]	P_{max}/A [mW/m ²]	Power conversion efficiency	Relative efficiency
10	0.0084	0.8362	0.1434	58.7311	0.00030	0.1228	0.00031	0.00108
20	0.0111	0.5566	0.2022	82.8443	0.00056	0.2306	0.00028	0.00056
30	0.0176	0.5866	0.3591	147.1143	0.00158	0.6472	0.00052	0.00086
40	0.0268	0.6708	0.6264	256.5886	0.00420	1.7213	0.00101	0.00151
50	0.0351	0.7029	0.8480	347.3498	0.00745	3.0520	0.00141	0.00198

The same trends for the 0.3M CuSO₄ 5H₂O based thermocell are observed as for the 0.1M CuSO₄ 5H₂O thermocell. Current density is again highest for $\Delta T = 50$ °C at $J_{sc} = 347.3498$ mA/m². Additionally, this is four and a half times higher than the current density at $\Delta T = 20$ °C and double the amount of the current density at $\Delta T = 30$ °C ($J_{sc} = 82.8443$ mA/m² and $J_{sc} = 147.1143$ mA/m², respectively). Maximum power output was also observed at $\Delta T = 50$ °C at $P_{max} = 0.00745$ mW with the corresponding current density of $P_{max}/A = 3.0520$ mW/m². The maximum power density doubled from increasing the temperature difference from $\Delta T = 40$ °C to $\Delta T = 50$ °C, (from $P_{max}/A = 1.7213$ mW/m² to

$P_{\max}/A = 3.0520 \text{ mW/m}^2$, respectively). Power conversion efficiency $\eta_{pc} = 0.00141 \%$ and relative efficiency $\eta_r = 0.00198 \%$ were also both highest at $\Delta T = 50 \text{ }^\circ\text{C}$.

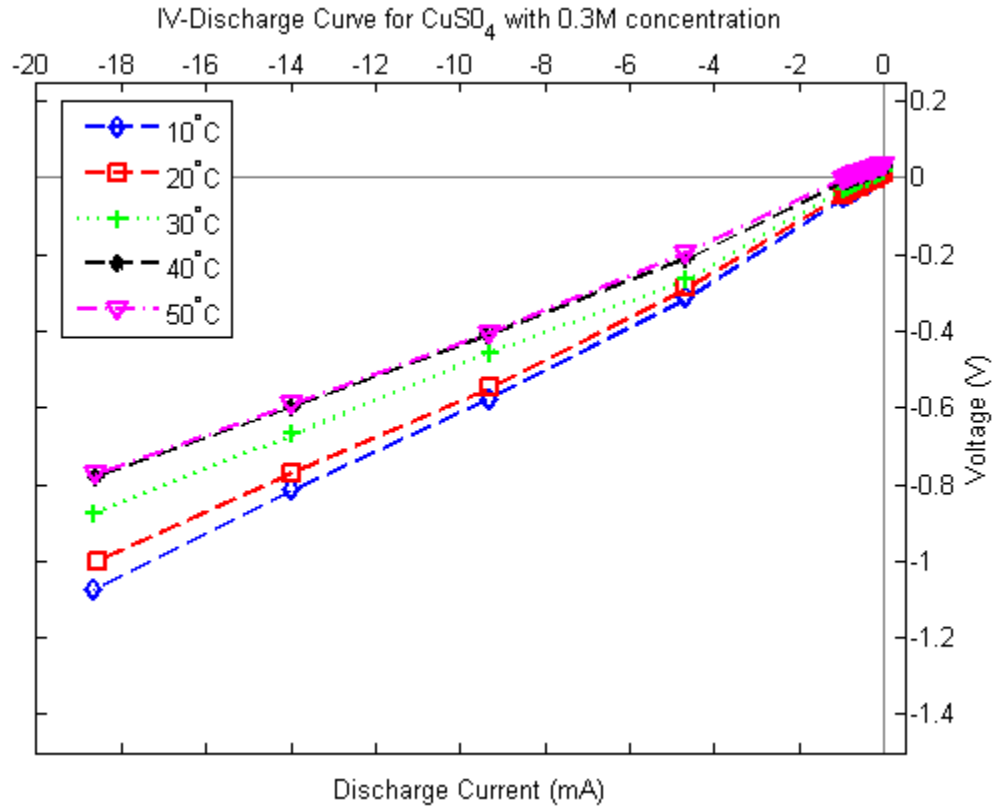


Figure 21. IV-Discharge Curve for 0.3M $\text{CuSO}_4 \cdot 5\text{H}_2\text{O}$ concentration and electrode separation of 6 in. for varying ΔT across the electrodes

From Table 3 it can be observed that the increased from $\Delta T = 30 \text{ }^\circ\text{C}$ to $\Delta T = 40 \text{ }^\circ\text{C}$ yields the biggest performance increase for the 0.3M $\text{CuSO}_4 \cdot 5\text{H}_2\text{O}$ based thermocell. Current density increases almost twofold, the power density triples, and the relative efficiency increases from $\eta_r = 0.00086 \%$ to $\eta_r = 0.00151 \%$. This is the highest increase in efficiency for any adjacent temperature gradients.

4. Characterization of 0.3M Copper II Sulfate Pentahydrate based three inch thermocell

The following study was conducted using a 0.3M Copper II Sulfate Pentahydrate electrolyte. But compared to the previous test the electrode spacing was decreased from six inches to three inches. Hence, electrolyte volume decreased from 0.5L to 150mL. Electrode surface area, however, was kept identical to the previous tests.

The maximum Seebeck coefficient to the 3 inches $\text{CuSO}_4 \cdot 5\text{H}_2\text{O}$ based thermogalvanic cell was measured at $\Delta T = 40^\circ\text{C}$ as $\alpha = 0.7478\text{ mV/K}$. This corresponds to an open circuit voltage of $V_{oc} = 0.0299\text{ V}$. The maximum observed open circuit voltage was $V_{oc} = 0.0342\text{ V}$ at $\Delta T = 50^\circ\text{C}$. The linear discharge curves suggest a constant Seebeck coefficient at around $\alpha = 0.6772\text{ mV/K}$. This is just slightly higher than the average Seebeck coefficient for the 6 inch electrode separation test cycle ($\alpha = 0.6706\text{ mV/K}$) with the same 0.3M $\text{CuSO}_4 \cdot 5\text{H}_2\text{O}$ electrolyte concentration. Open circuit voltages also remained almost constant for both tests. Small differences can be attributed to slight changes in convective behavior but overall concentration is a major factor for thermogalvanic cell performance.

Table 4Characterization of 0.3M Copper II Sulfate Pentahydrate based 3 inch thermocell

ΔT [°C]	E_{oc} [V]	α [mV/K]	I_{sc} [mA]	J_{sc} [mA/m ²]	P_{max} [mW]	P_{max}/A [mW/m ²]	Power conversion efficiency	Relative efficiency
10	0.0068	0.6822	0.1025	41.9985	0.00017	0.0716	0.00009	0.00031
20	0.0133	0.6644	0.2166	88.7041	0.00072	0.2947	0.00018	0.00036
30	0.0182	0.6071	0.3357	137.5174	0.00153	0.6262	0.00025	0.00042
40	0.0299	0.7478	0.6152	251.9955	0.00460	1.8844	0.00055	0.00083
50	0.0342	0.6844	0.7440	304.7664	0.00637	2.6075	0.00060	0.00085

Power and current densities again increased with an increase in temperature gradient. The maximum current density was observed at $\Delta T= 50$ °C as $J_{sc}= 304.7664$ mA/m². The highest power output was again at $\Delta T= 50$ °C, $P_{max}= 0.00637$ mW. Thus, the analogous power density is 2.6075 mW/m². The biggest increase in performance for this thermocell is documented when the temperature gradient between the two electrodes is increased from $\Delta T= 30$ °C to $\Delta T= 40$ °C. Current and power densities increase about four times and the maximum power increases about threefold from $P_{max}= 0.00153$ V to $P_{max}= 0.00460$ mW.

The maximum power conversion efficiency is also at $\Delta T= 50$ °C of $\eta_{pc}= 0.00060$ % and a corresponding relative efficiency of $\eta_r= 0.00085$ %. Once again, as in the 0.1M CuSO₄ 5H₂O test, the relative efficiency does not increase for a specific temperature increase. When the temperature is increased from $\Delta T= 40$ °C to $\Delta T= 50$ °C the relative efficiency stays the same ($\eta_r= 0.00083$ % to $\eta_r= 0.00085$ %, respectively.) The maximum

possible power density output of the thermocell, however, almost doubles for the same temperature gradient increase from $P_{\max}/A= 1.8844 \text{ mW/m}^2$ to $P_{\max}/A= 2.6075 \text{ mW/m}^2$.

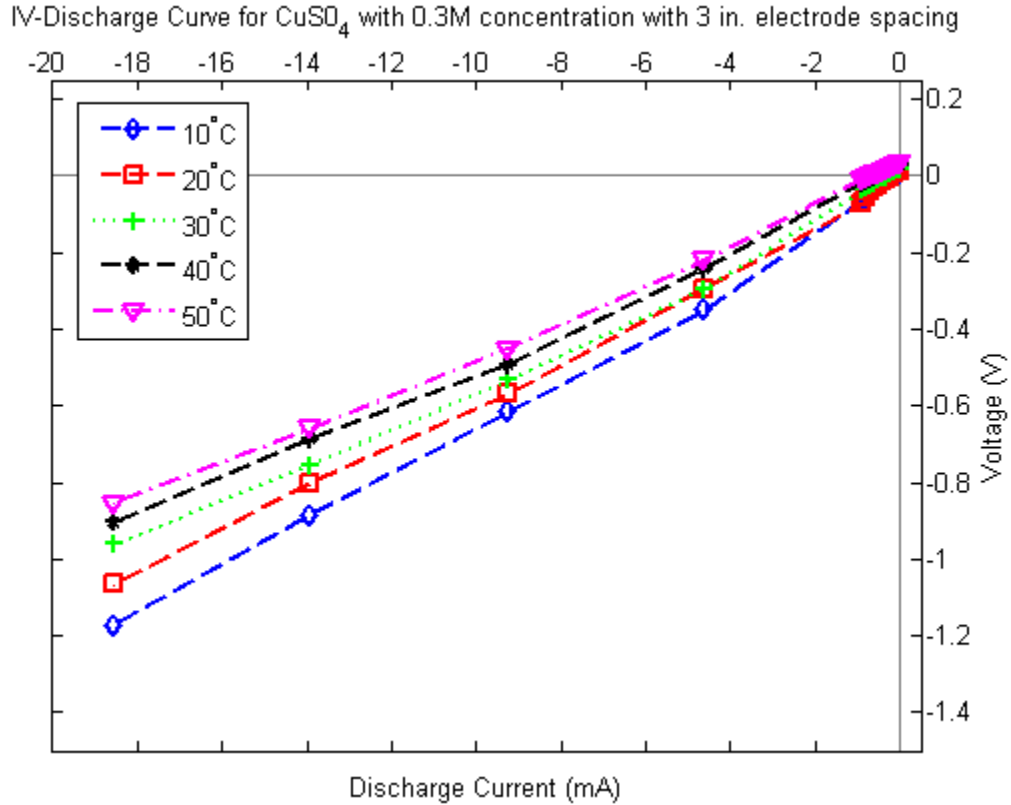


Figure 22. IV-Discharge Curve for 0.3M $\text{CuSO}_4 \cdot 5\text{H}_2\text{O}$ concentration and electrode separation of 3 in. for varying ΔT across the electrodes

5. Characterization of 0.3M Copper II Sulfate Pentahydrate based two inch thermocell

The following experiment was conducted using a 0.3M Copper II Sulfate Pentahydrate electrolyte with electrode spacing of 2 inches. The electrolyte volume was reduced to 100 mL but the electrode surface area was kept the same for accurate comparison of the different test cases.

The maximum open circuit voltage measured was $V_{oc} = 0.0324$ V. The open circuit ranged from $V_{oc} = 0.0068$ V to $V_{oc} = 0.0324$ V for $\Delta T = 10$ °C -50 °C. The highest measured Seebeck coefficient $\alpha = 0.7324$ mV/K at $\Delta T = 40$ °C. Since the IV-Discharge curve exhibits linear behavior the Seebeck coefficient is constant, averaging the coefficient over all temperature gradients it comes out to around $\alpha = 0.6606$ mV/K. This is slightly lower than the Seebeck coefficient for both the 0.3M $\text{CuSO}_4 \cdot 5\text{H}_2\text{O}$ based thermocell with six inch and three inch electrode separation ($\alpha = 0.6706$ mV/K and $\alpha = 0.6772$ mV/K, respectively). Open circuit voltages are virtually identical for the two inch and three inch test cycle and slightly higher for six inch test ($V_{oc} = 0.0342$ V for two and three inches each and $V_{oc} = 0.0351$ V).

Table 5

Characterization of 0.3M Copper II Sulfate Pentahydrate based 2 inch thermocell

ΔT [°C]	E_{oc} [V]	α [mV/K]	I_{sc} [mA]	J_{sc} [mA/m ²]	P_{max} [mW]	P_{max}/A [mW/m ²]	Power conversion efficiency	Relative efficiency
10	0.0068	0.6822	0.1126	59.1235	0.00019	0.1008	0.00008	0.00029
20	0.0133	0.6644	0.2210	116.0216	0.00073	0.3854	0.00016	0.00031
30	0.0173	0.5763	0.3439	180.5557	0.00149	0.7804	0.00021	0.00035
40	0.0293	0.7324	0.6638	348.5667	0.00486	2.5529	0.00050	0.00075
50	0.0336	0.6720	0.7378	387.4142	0.00597	3.1356	0.00048	0.00068

For this thermocell setup the maximum recorded current density was $J_{sc} = 387.4142$ mA/m² at $\Delta T = 50$ °C. The resulting maximum power output for the thermocell

is $P_{\max} = 0.00597 \text{ mW}$ which is equal to a peak power density of $P_{\max}/A = 3.1356 \text{ mW/m}^2$.

Increasing the temperature gradient from $\Delta T = 30 \text{ }^\circ\text{C}$ to $\Delta T = 40 \text{ }^\circ\text{C}$ yielded the biggest performance increase. The maximum power density increased by three times from $P_{\max}/A = 0.7804 \text{ mW/m}^2$ to $P_{\max}/A = 2.5529 \text{ mW/m}^2$.

Relative and power conversion efficiencies were both largest at $\Delta T = 40 \text{ }^\circ\text{C}$ at $\eta_r = 0.00075 \%$ and $\eta_{pc} = 0.00050 \%$, respectively. The maximum relative efficiency for the two inch separation test is slightly lower than for the $0.3\text{M CuSO}_4 \cdot 5\text{H}_2\text{O}$ based thermocell with a three inch electrode spacing ($\eta_r = 0.00085 \%$). The identical electrolyte based thermocell with a six inch electrode separation had a relative efficiency around three times higher than the two inch separation ($\eta_r = 0.00198 \%$).

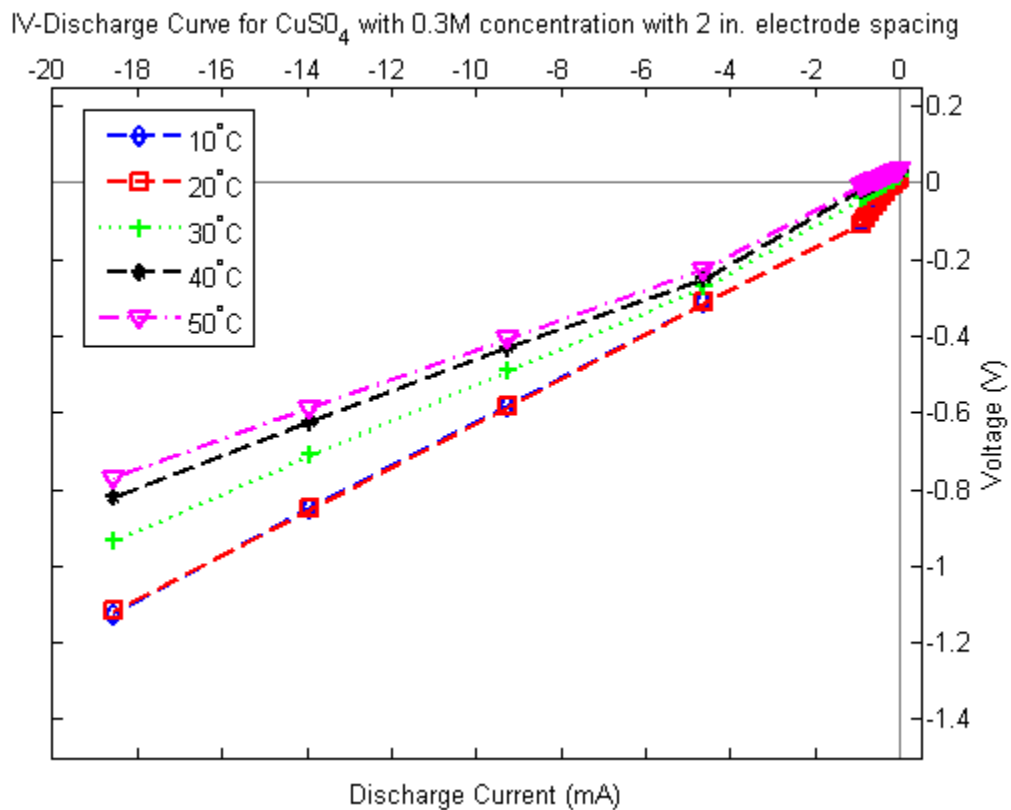


Figure 23. IV-Discharge Curve for $0.3\text{M CuSO}_4 \cdot 5\text{H}_2\text{O}$ concentration and electrode separation of 2 in. for varying ΔT across the electrodes

6. Characterization of 0.3M Copper II Sulfate Pentahydrate based three inch thermocell with 0.00183 m² electrode surface area

The following two tests were conducted using the modified thermocell setup with three inch electrode separation. During both tests parts of the copper electrodes were covered with silicone to decrease the surface area. The concentration for both tests was set at 0.3M CuSO₄ 5H₂O.

The average Seebeck coefficient for this test run was at $\alpha = 0.6548$ mV/K with all the IV-Discharge curves exhibiting linear behavior. Open circuit voltage was maximum at $\Delta V_{oc} = 0.03453$ V where the temperature gradient was at $\Delta T = 50$ °C. Thus, the Seebeck coefficient is slightly lower than the test with the greater electrode surface area, $\alpha = 0.6772$ mV/K with $A = 0.00244$ m². The maximum open circuit voltages are almost identical, $\Delta V_{oc} = 0.03453$ V and $\Delta V_{oc} = 0.0342$ V, both at $\Delta T = 50$ °C, which can be attributed to small errors in the temperature difference.

Table 6

Characterization of 0.3M Copper II Sulfate Pentahydrate based 3 inch thermocell with 0.00183 m² electrode surface area

ΔT [°C]	E_{oc} [V]	α [mV/K]	I_{sc} [mA]	J_{sc} [mA/m ²]	P_{max} [mW]	P_{max}/A [mW/m ²]	Power conversion efficiency	Relative efficiency
10	0.00682	0.6822	0.1069	58.4054	0.00018	0.0996	0.00012	0.00044
20	0.01206	0.6028	0.1847	100.9226	0.00056	0.3042	0.00019	0.00037
30	0.01883	0.6276	0.3231	176.5728	0.00152	0.8312	0.00033	0.00055
40	0.02683	0.6708	0.4925	269.1192	0.00330	1.8054	0.00053	0.00079
50	0.03453	0.6906	0.7255	396.4551	0.00626	3.4224	0.00079	0.00111

The maximum short circuit current density was recorded at $\Delta T = 50$ °C at $J_{sc} = 396.4551$ mA/m². At the same temperature gradient the maximum power out was also largest at $P_{max} = 0.00626$ mW. This corresponds to a maximum power density of $P_{max}/A = 3.4224$ mW/m². Thus the maximum power is lower compared to the 0.3M CuSO₄ 5H₂O test with surface area at $A = 0.00244$ m² ($P_{max} = 0.00637$ mW). The maximum power density has slightly increased however from $P_{max}/A = 2.6075$ mW/m² to $P_{max}/A = 3.4224$ mW/m².

Power conversion efficiency and relative efficiency were both highest at $\Delta T = 50$ °C, ($\eta_{pc} = 0.00079$ % and $\eta_r = 0.00111$ %). Thus the efficiency is slightly better for this cell than compared to the same cell with a bigger electrode surface area, ($\eta_{pc} = 0.00060$ % and $\eta_r = 0.00085$ %).

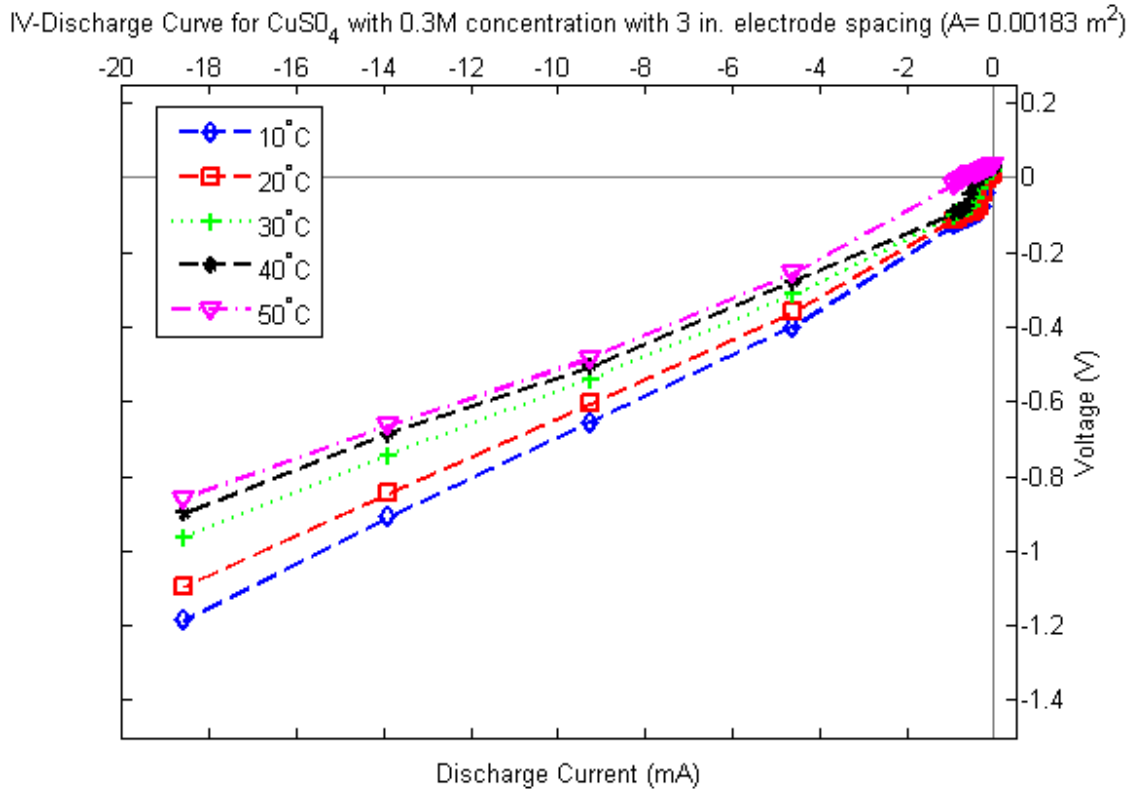


Figure 24. IV-Discharge Curve for 0.3M $\text{CuSO}_4 \cdot 5\text{H}_2\text{O}$ concentration and electrode separation of 3 in. with electrode surface area of $A= 0.00183 \text{ m}^2$ for varying ΔT across the electrodes.

7. Characterization of 0.3M Copper II Sulfate Pentahydrate based three inch thermocell with 0.00144 m^2 electrode surface area

This test was run with the conditions described in the previous section. The major change was reducing the electrode surface area from $A= 0.00183 \text{ m}^2$ to $A= 0.00144 \text{ m}^2$ to study the effect of changing electrode surface area on thermocell power production.

For this thermocell setup the maximum open circuit voltage was measured at $\Delta T = 50 \text{ }^\circ\text{C}$ as $\Delta V_{oc} = 0.03422\text{V}$. This also coincided with the maximum Seebeck coefficient of $\alpha= 0.6844 \text{ mV/K}$. Due to the linearity of the IV-Discharge curve the Seebeck

coefficient is assumed to be constant at $\alpha = 0.6476$ mV/K. This is lower than for the tests with an electrode area of $A = 0.00183$ m² and $A = 0.0244$ m² ($\alpha = 0.6548$ mV/K and $\alpha = 0.6772$ mV/K, respectively). The open circuit voltage is very stable for the tests with smaller surface area around $\Delta V_{oc} = 0.0342$ V and just slightly higher for the original setup at $\Delta V_{oc} = 0.0345$ V.

Table 7

Characterization of 0.3M Copper II Sulfate Pentahydrate based 3 inch thermocell with 0.00144 m² electrode surface area

ΔT [°C]	E_{oc} [V]	α [mV/K]	I_{sc} [mA]	J_{sc} [mA/m ²]	P_{max} [mW]	P_{max}/A [mW/m ²]	Power conversion efficiency	Relative efficiency
10	0.00665	0.6650	0.1093	75.9357	0.00018	0.1262	0.00016	0.00055
20	0.01236	0.6182	0.1196	83.0511	0.00037	0.2567	0.00016	0.00031
30	0.01914	0.6379	0.3246	225.4045	0.00155	1.0784	0.00043	0.00072
40	0.02529	0.6324	0.5032	349.4251	0.00318	2.2096	0.00065	0.00097
50	0.03422	0.6844	0.7072	491.0923	0.00605	4.2016	0.00097	0.00136

The maximum power produced for this thermogalvanic cell setup was measured at $\Delta T = 50$ °C as $P_{max} = 0.00605$ mW, corresponding to a maximum current density of $P_{max}/A = 4.2014$ mW/m². The short circuit current density was also maximum at the same temperature difference ($J_{sc} = 491.0923$ mA/m²). The maximum power output is again lower than the two other comparable tests ($P_{max} = 0.00626$ mW for $A = 0.00183$ m² and $P_{max} = 0.00637$ mW for $A = 0.0244$ m²). Another increase in maximum power density

was noticed. For the $A= 0.00244 \text{ m}^2$ test $P_{\max}/A= 2.6075 \text{ mW/m}^2$, for $A= 0.00183 \text{ m}^2$ $P_{\max}/A= 3.4224 \text{ mW/m}^2$ and for the current the $A= 0.00144 \text{ m}^2$ $P_{\max}/A= 4.2016 \text{ mW/m}^2$.

Power conversion efficiency and relative efficiency were maximum at $\Delta T = 50 \text{ }^\circ\text{C}$ and calculated to be $\eta_{pc}= 0.00097 \%$ and $\eta_r= 0.00136 \%$). Again, a slightly increase in both power conversion and relative efficiency is noticed compared to the previous tests. For the $A= 0.00183 \text{ m}^2$ test the efficiencies were around 22 % lower than the current test (relative efficiency increased from $\eta_r= 0.00111 \%$ to $\eta_r= 0.00136 \%$).

IV-Discharge Curve for CuSO_4 with 0.3M concentration with 3 in. electrode spacing ($A= 0.00144 \text{ m}^2$)

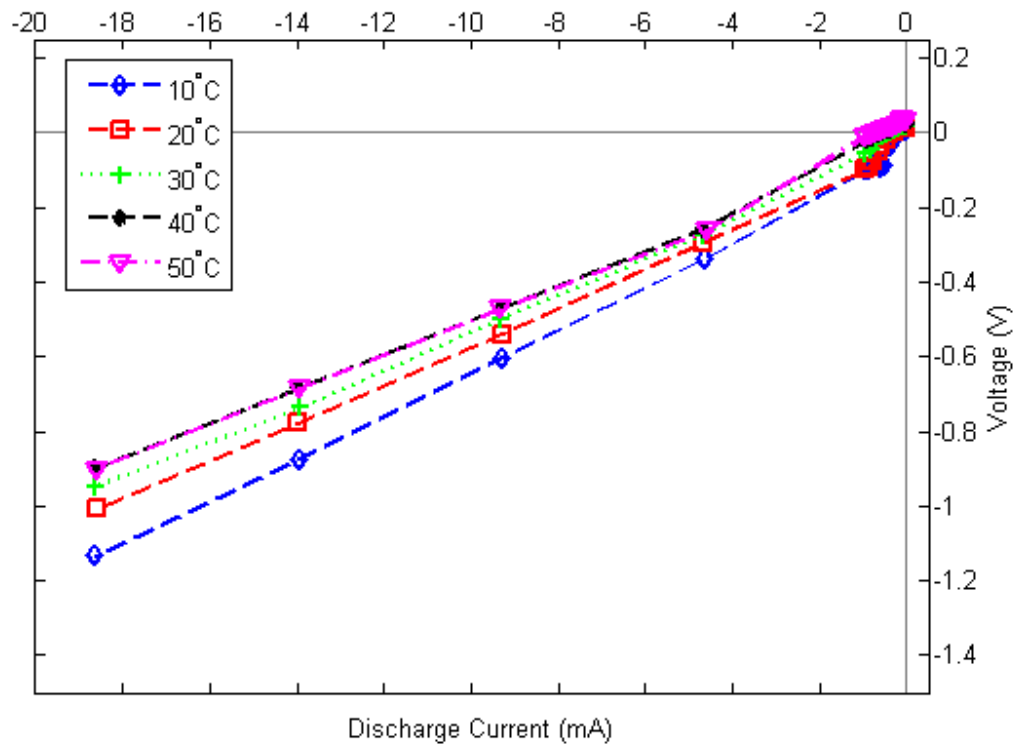


Figure 25. IV-Discharge Curve for 0.3M $\text{CuSO}_4 \cdot 5\text{H}_2\text{O}$ concentration and electrode separation of 3 in. with electrode surface area of $A= 0.00144 \text{ m}^2$.

8. Power dependence on electrolyte concentration

The following figure compares the maximum power output for a Copper II Sulfate Pentahydrate thermogalvanic cell with difference electrolyte concentrations. The electrode spacing is always at $d= 6$ inches and the temperature difference is at $\Delta T= 50$ °C. The electrode surface area is also kept constant.

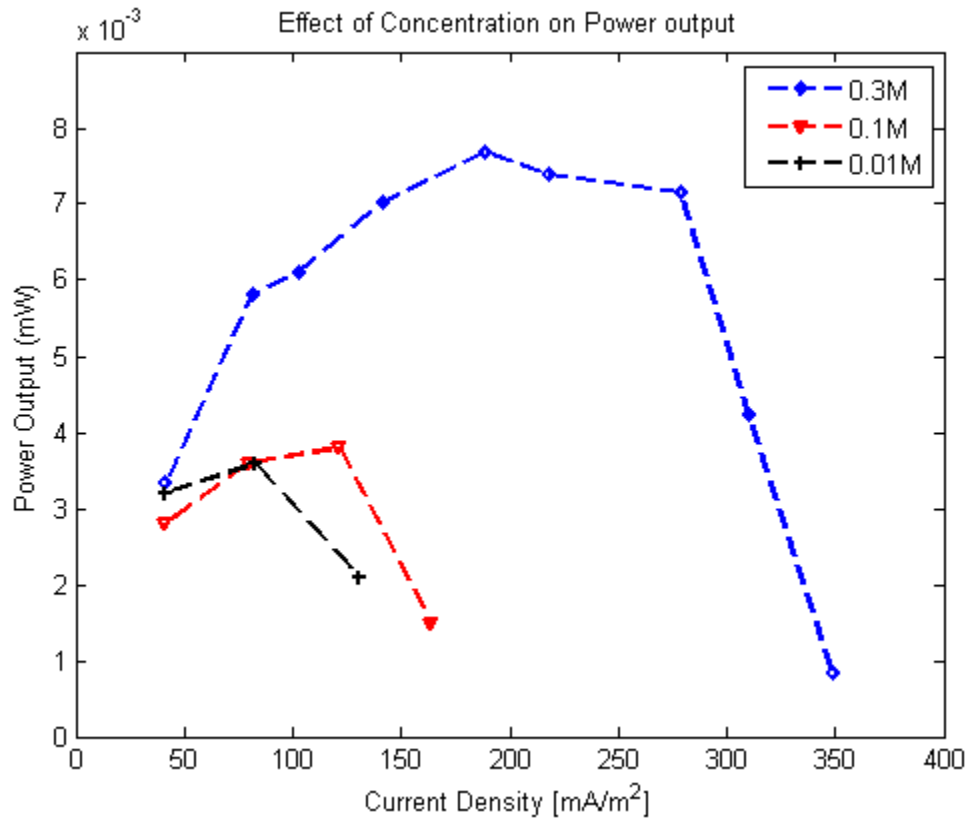


Figure 26. Power Output depending on Electrolyte Concentration plotted versus current density (all test cycles were conducted at $\Delta T=50$ °C).

The figure shows that an increase in electrolyte concentration will lead to an increase in maximum power output. When the concentration is increased from 0.01M to 0.1M $\text{CuSO}_4 \cdot 5\text{H}_2\text{O}$ the maximum power increases slightly. There is a very large increase, however, when the concentration is increased from 0.1M to 0.3M. The power output

actually doubles for the corresponding concentration increase. Additionally, the range of high power output is larger for higher concentrations. Whereas for the low concentrations (0.01M and 0.1M) there is only a small current density band where there is a large power output, the 0.3M $\text{CuSO}_4 \cdot 5\text{H}_2\text{O}$ thermocell has high power outputs for significantly larger range.

9. Power dependence on electrode spacing

The following figure compares the maximum power output for a Copper II Sulfate Pentahydrate thermogalvanic cell with changing electrode separation distances. The electrode concentration is always at 0.3M $\text{CuSO}_4 \cdot 5\text{H}_2\text{O}$ and the temperature difference is at $\Delta T = 50^\circ\text{C}$. The electrode surface area is also kept constant.

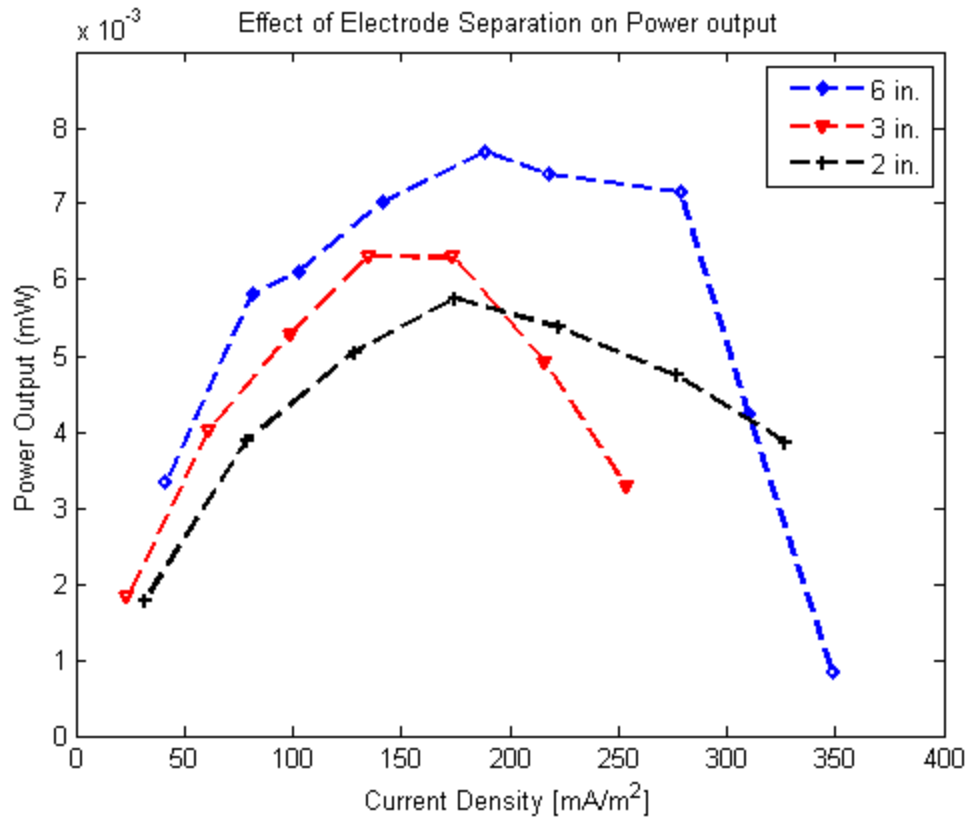


Figure 27. Power dependence on electrode spacing plotted versus current density (all test cycles were conducted at $\Delta T=50\text{ }^{\circ}\text{C}$).

Here the graph shows that with increasing electrode distance the maximum power output also increases. The six inch electrode spaced thermocell has the greatest output overall. However, electrode spacing effects on performance are not as severe as a change in electrolyte, as seen in the previous Figure 26. The two inch thermocell has a large current density band of high power output but the maximum is lower than for the three inch thermocell which has the smallest range of power output.

The following figure compares the internal resistance and the relative efficiency for different electrode separations. All thermocells were tested with 0.3M $\text{CuSO}_4 \cdot 5\text{H}_2\text{O}$.

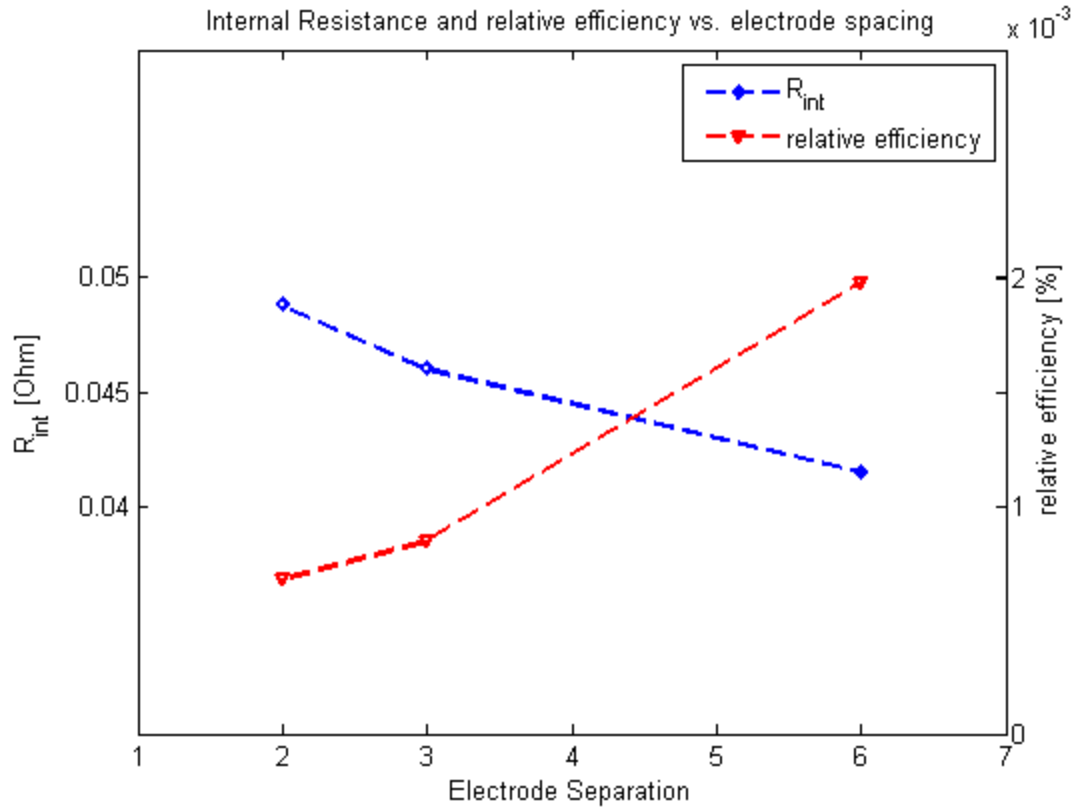


Figure 28. Electrode spacing effects on relative efficiency and internal resistance (at P_{max} and $\Delta T= 50\text{ }^{\circ}\text{C}$).

The internal resistance decreases linearly with an increase in electrode spacing. This is expected since the maximum power output went up for an increase in separation. Since the $\text{CuSO}_4 \cdot 5\text{H}_2\text{O}$ electrolyte has a linear behavior this behavior is expected to hold for any larger increase in electrode separation.

The relative efficiency did also increase with an increase in electrode separation. The increase is also fairly linear; however, the jump in relative efficiency from two to three inch spacing was rather small. The relative efficiency doubled when the electrode spacing was increased from three to six inches. This trend is also expected to be stable when looking at the power conversion and relative efficiency equations (Eqn. 14 and 15).

10. Power dependence on electrode surface area

In the subsequent figure the effect of electrode surface area on power production for a Copper II Sulfate Pentahydrate thermogalvanic cell is shown. All test cycles were ran with the same concentration of 0.3M $\text{CuSO}_4 \cdot 5\text{H}_2\text{O}$ and a temperature gradient of $\Delta T = 50\text{ }^\circ\text{C}$. The electrode spacing is kept constant at three inches.

The graph shows that with increasing electrode surface area power production increases favorably (P_{max} increases). This is most likely due to the fact that more electrode reaction sites are available for the redox reaction to take place. The effect is not as profound, however, as a change in the concentration or a change in electrode spacing. In fact, a 40 % reduction in electrode surface area (from $A = 0.00244\text{ m}^2$ to $A = 0.00144\text{ m}^2$) reduced the maximum power output only by five percent.

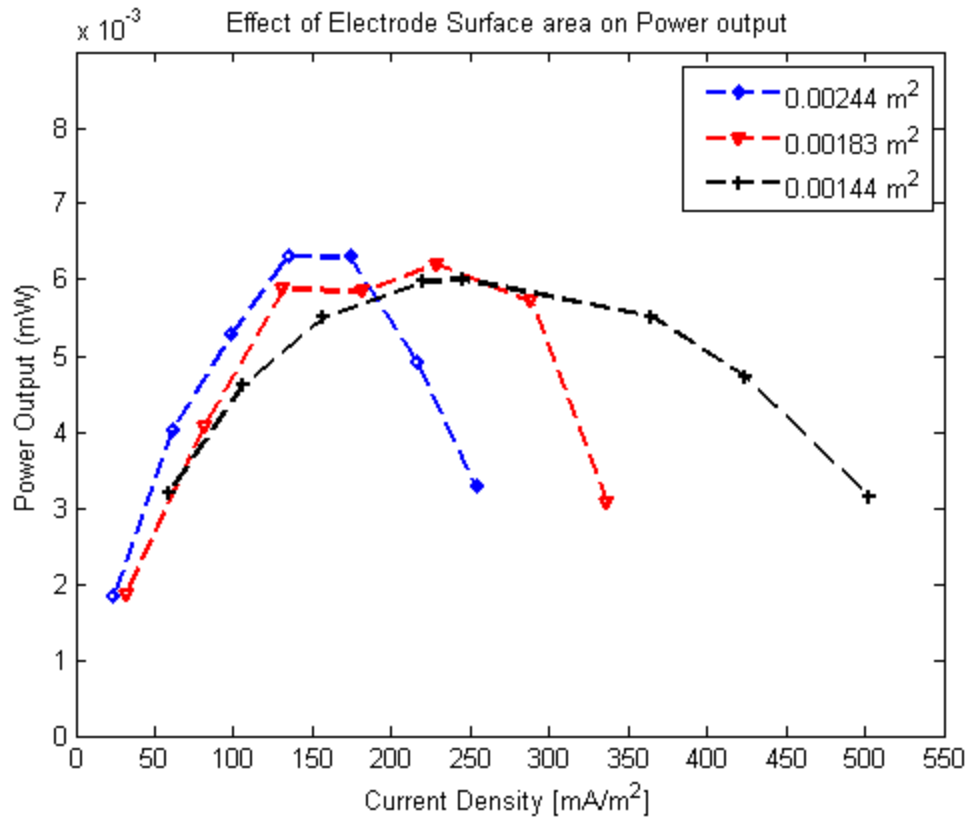


Figure 29. Power dependence on electrode surface area plotted versus current density (all test cycles were conducted at $\Delta T=50\text{ }^{\circ}\text{C}$).

Another noticeable effect was that the current density range increased with decreased electrode surface area. Thus power could be produced over a larger range of discharge currents for a cell with a smaller electrode surface area. This has the effect that power density actually increases as the electrode surface area goes down. Since the surface area is a factor for calculating the power conversion efficiency for a thermogalvanic cell, efficiency also increases as shown in the next figure.

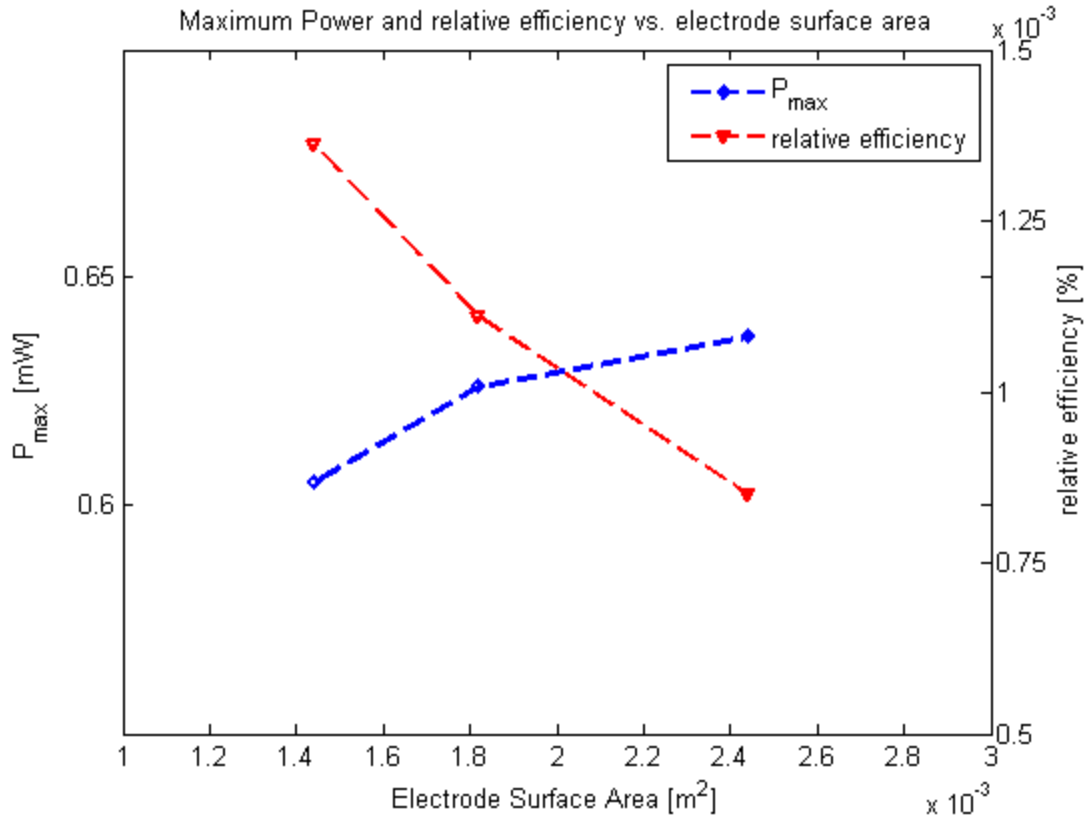


Figure 30. Electrode surface area effects on relative efficiency and maximum power output ($d= 3$ inches and $\Delta T= 50$ °C).

Thus a thermogalvanic cell electrode surface area should be designed so that the operating condition maximizes efficiency yet still outputs a desired amount of power. Since the surface area does not have the largest impact on maximum power production it would be more important to consider first the concentration and electrode spacing before accommodating the design for an adjustment in electrode spacing.

B. Heat transfer in a thermogalvanic cell

Due to the temperature gradient between the two electrodes in a thermogalvanic cell, heat transfer can affect the performance of a thermocell. The heat transfer from the hot electrode to the cold electrode and hence a reduction in temperature difference will lead to a performance reduction. The following equation shows the direct dependence of performance to the thermal conductivity of an electrolyte material.

$$\eta_{pc} = \frac{P_{max}}{kA \left(\frac{\partial T}{\partial x} \right)} \quad (14)$$

With increasing thermal conductivity the performance of a thermogalvanic cell decreases. Thus, a good electrolyte material will have advantageous thermal conductivity properties.

The importance of low thermal conductivity stem from the application of thermogalvanic cells. Since the primary target use are low waste heat energy sources such as piping in power plants or automobiles, the cold electrode side will only be cooled by the ambiance. Since ambient temperatures for thermocell applications are pretty constant, excessive heat transfer can drastically decrease the performance of a thermocell. In the previous section the profound impact of temperature gradients on thermocell performance was noted.

Experiments conducted in the current study had constant cooling of the cold electrode side to maintain the temperature difference. This was done to accurately measure and compare performance characteristic for different setups. This is of course a

non ideal, cost-ineffective way for a commercial application. The following thermal images of running experiments were taken to view the temperature profile of a thermocell.

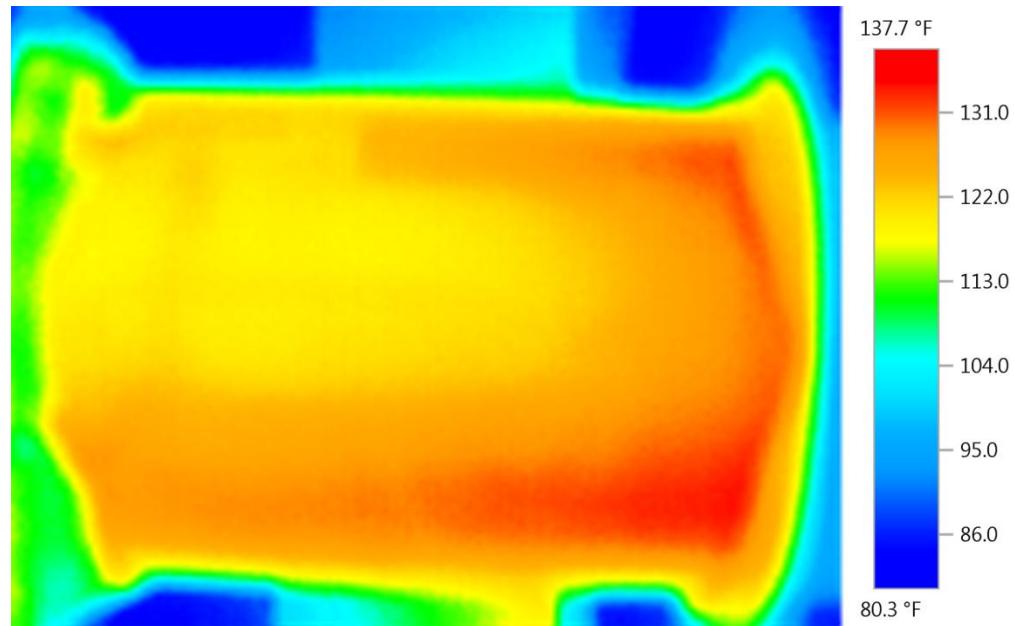


Figure 31. Thermal image for 0.3M $\text{CuSO}_4 \cdot 5\text{H}_2\text{O}$ based thermocell test with the hot electrode side at $T= 60^\circ\text{C}$ and the cold electrode at ambient temperature ($T= 23^\circ\text{C}$).

The hottest temperature areas are at the top and bottom of the hot electrode side. As Gunawan et al. noted, this could arise from the effect of natural convection aiding the thermocell's performance and ion flow (Gunawan et al., 2014).

1. SolidWorks Simulation of Heat flow

SolidWorks Flow Simulation was used to simulate the heat flow throughout the thermocell based on a given electrolyte. The electrolyte used in the current study has a thermal conductivity of $\kappa= 0.6575 \text{ W}/(\text{m}\cdot\text{K})$ for $\Delta T= 70^\circ\text{C}$ and 0.3M $\text{CuSO}_4 \cdot 5\text{H}_2\text{O}$ (Aseyev, 1992). For the simulation two copper endplates and the glass cell were modeled.

Then initial and boundary conditions were applied and the heat convective flow was simulated.

a. Initial and Boundary Conditions

Both copper electrode plates were set to a constant temperature ($T= 20\text{ }^{\circ}\text{C}$ and $T= 70\text{ }^{\circ}\text{C}$) and the electrolyte started also at ambient temperature ($T= 20\text{ }^{\circ}\text{C}$.) In other words the constant temperature simulated the constant cooling and heating of the electrodes and the electrolyte was allowed to warm up. Heat transfer coefficients were picked from the SolidWorks material library. Tables were used to get the thermal conductivity coefficient for Copper II Sulfate Pentahydrate (Aseyev, 1992). The electrolyte started out at rest and no flow velocity was applied. Laminar flow was assumed throughout the electrolyte.

First an idealized cell of one centimeter length and diameter was simulated to ensure accuracy of the results. Then the assembly was modified to the experimental dimensions of six inches in length and two inches in diameter. The SI unit system was used in the simulation. The simulation ran for 1800 seconds and an automatic, semi-fine mesh was applied to the cell assembly.

b. Simulation Results

The following figures show the idealized temperature gradient throughout the electrolyte and flow patterns because of the natural convection.

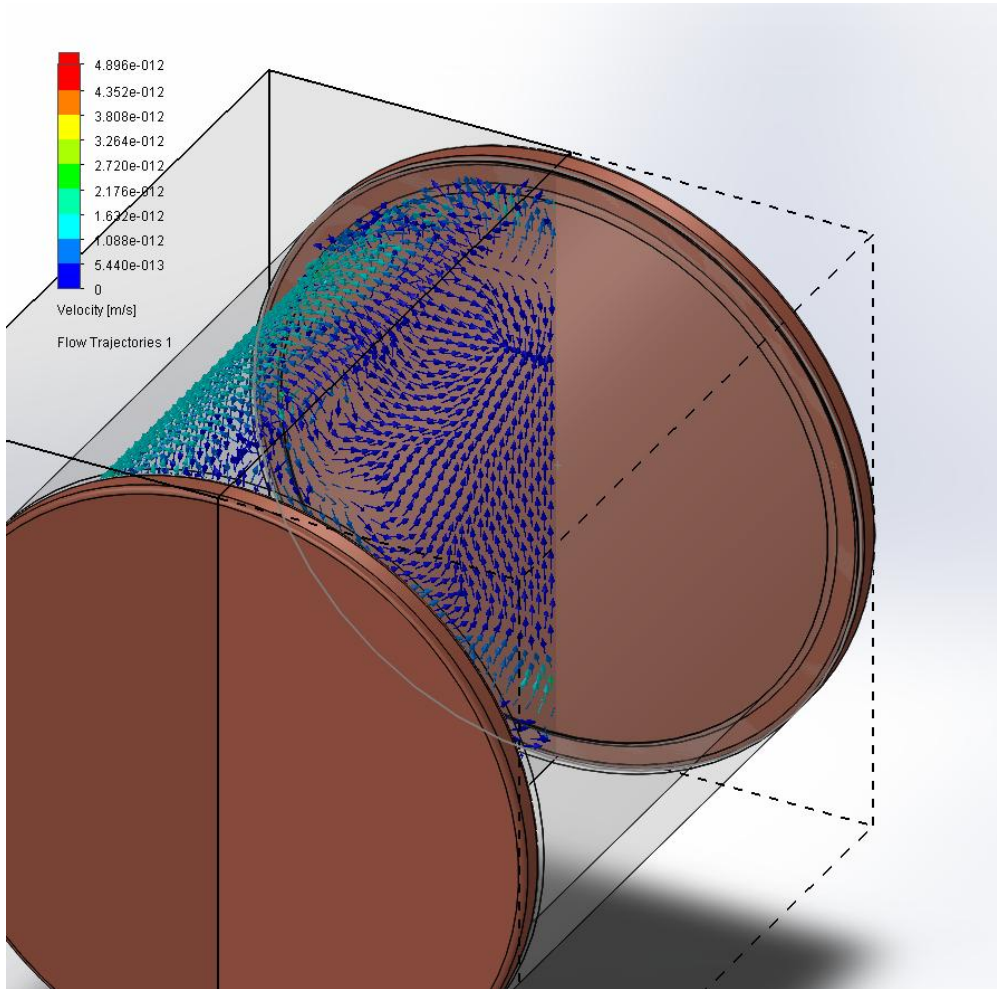


Figure 32. Flow velocities shown on the hot electrode side caused by natural heat convection in the thermocell.

The simulated flow patterns pictured in Figure 32 are indicative of the actual behavior observed in the experiment and show by the thermal image in Figure 31. Heat flow is in the upward direction on the thermocell moving the electrolyte from the bottom to the top and thus supporting ion flow. The experiment also shows higher temperature at

the bottom and the top of the hot electrode. In the heat flow simulation small circulations of electrolyte flow are shown at the cell electrode interface but the flow is very uniform at the center of the electrode.

The following temperature distributions for the different simulation setups show the temperature gradient of the electrolyte after 1800s. The electrolyte is modeled as an idealized fluid and other effects such as mass or ion movements are ignored. Only heat transfer effects due to the temperature difference between the two electrodes were considered. Hence, the figures show a very uniform distribution which is not the actual behavior. These graphs can still be used to detract important information about the design of a thermocell. Electrode spacing should be chosen carefully such that heat flow will not heat up the cold electrode more than a few degrees.

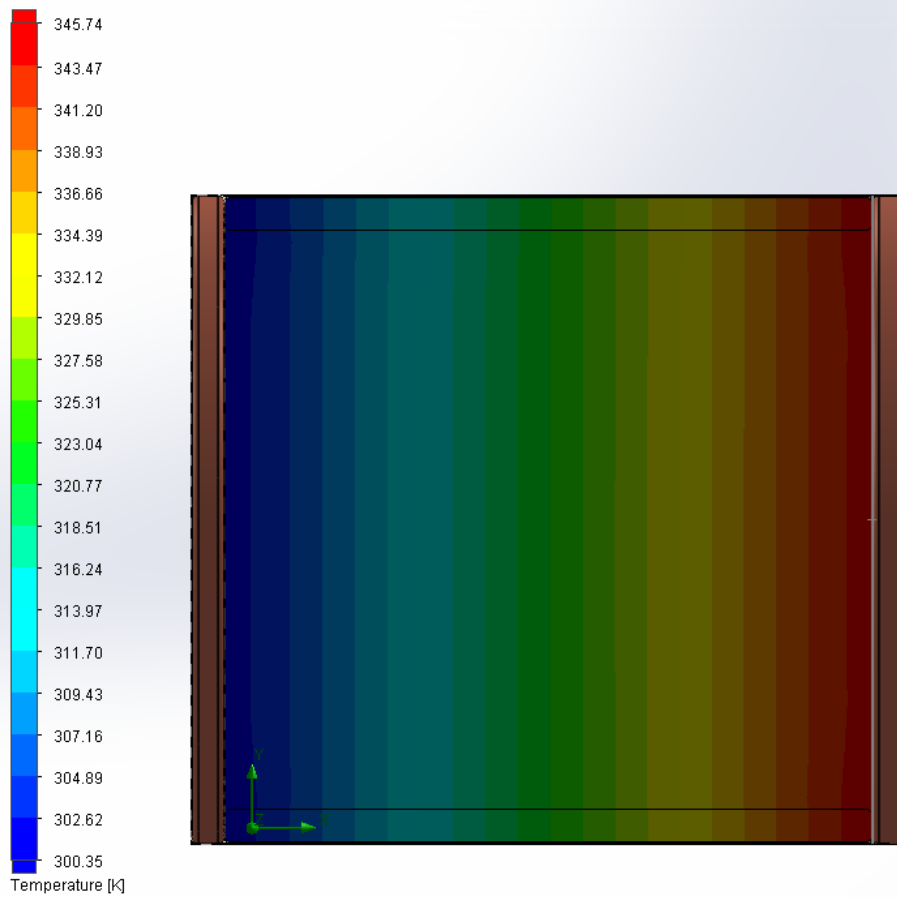


Figure 33. Temperature distribution for the small one centimeter length $\text{CuSO}_4 \cdot 5\text{H}_2\text{O}$ thermocell after 1800 seconds.

For both Figure 33 and Figure 34 the maximum and minimum temperatures are identical due to the idealized electrolyte simulation. The electrolyte heats up to almost $T = 40^\circ\text{C}$ on the cold side after 1800 seconds even when keeping the copper plate at a constant $T = 20^\circ\text{C}$. The warm side is still getting heated up to being at the set temperature of $T = 70^\circ\text{C}$.

In Figure 34, the test-sized simulation, it can be observed that the hot to cold transition does not occur in the middle of the glass cell as it does for the one centimeter

thermocell. The transition region is very close to the hot electrode side at around one quarter of the total thermocell length. Since this is a snapshot at 1800 seconds into the simulation it is expected that the thermocell temperature distribution would look similar to Figure 33 when simulation time is increased. This suggests that by increasing electrode spacing heat transfer throughout the thermocell will be slowed down. Hence, the temperature gradient will stay higher for a longer period. The ion movement however, will be slowed down when increasing the distance and thus optimal spacing for the electrodes should be determined to have maximum performance (Salazar, Kumar, & Cola, 2014).

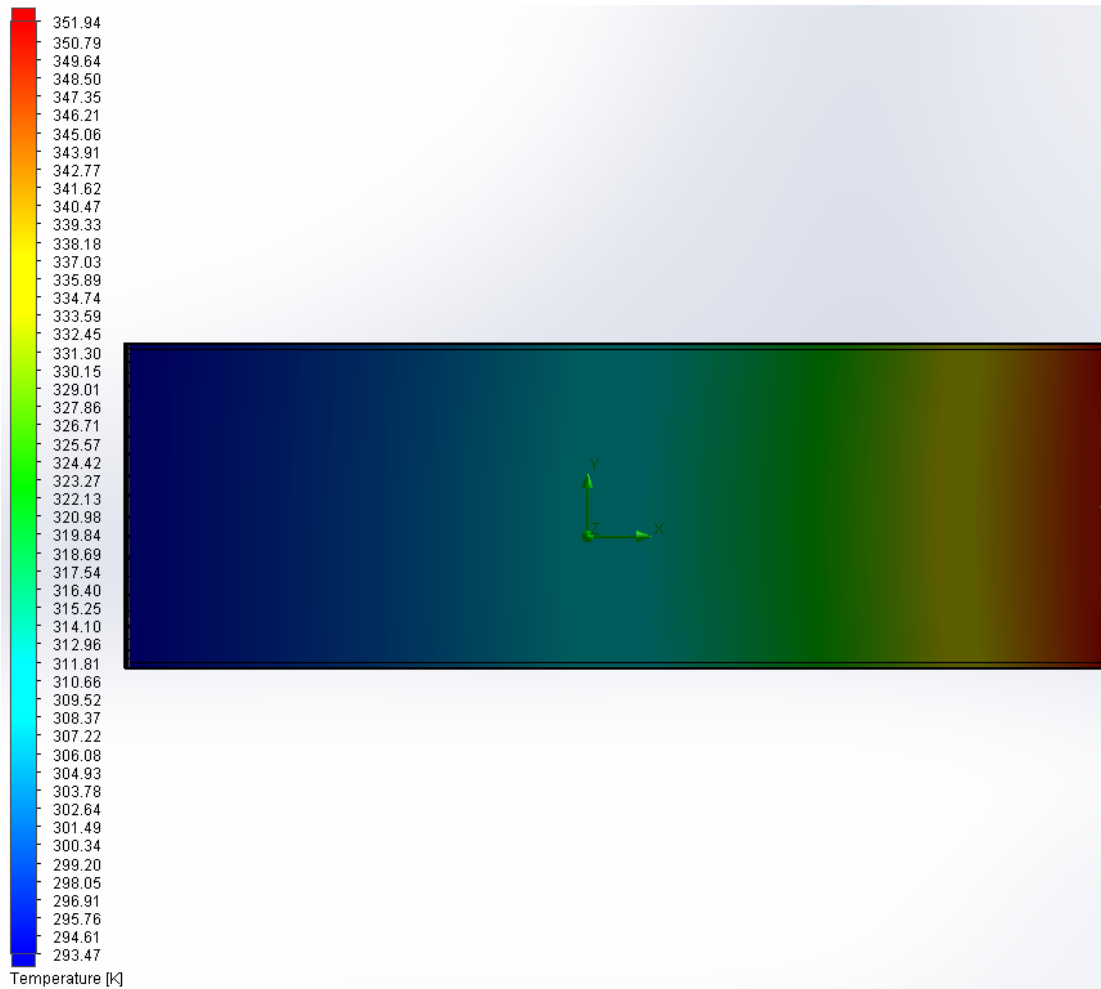


Figure 34. Temperature distribution for the six inch $\text{CuSO}_4 \cdot 5\text{H}_2\text{O}$ thermocell after 1800 seconds.

Figure 35 compares the temperature distributions of a thermocell (with electrode spacing $d=6$ inches) at different times throughout a testing cycle. Part a shows the cell temperature distribution after 900 seconds. At this point the hot region of the electrolyte is rather small. In parts b and c the hot region gets bigger because of the heat conduction from the hot copper electrode. In part d, after two hours or 7200 seconds, the warm regions of the electrolyte are significantly bigger compared to part a.

If the test were run for longer than two hours, it is expected that a similar temperature distribution as Figure 33 is expected for the simulation with six inches of electrode spacing. The heat gradient should be uniform throughout a thermocell if the temperature difference is applied for long enough time. Hence, larger electrode spacing will prevent fast heat transfer and the thermogalvanic cell will run longer at an optimum temperature difference without need external cooling.

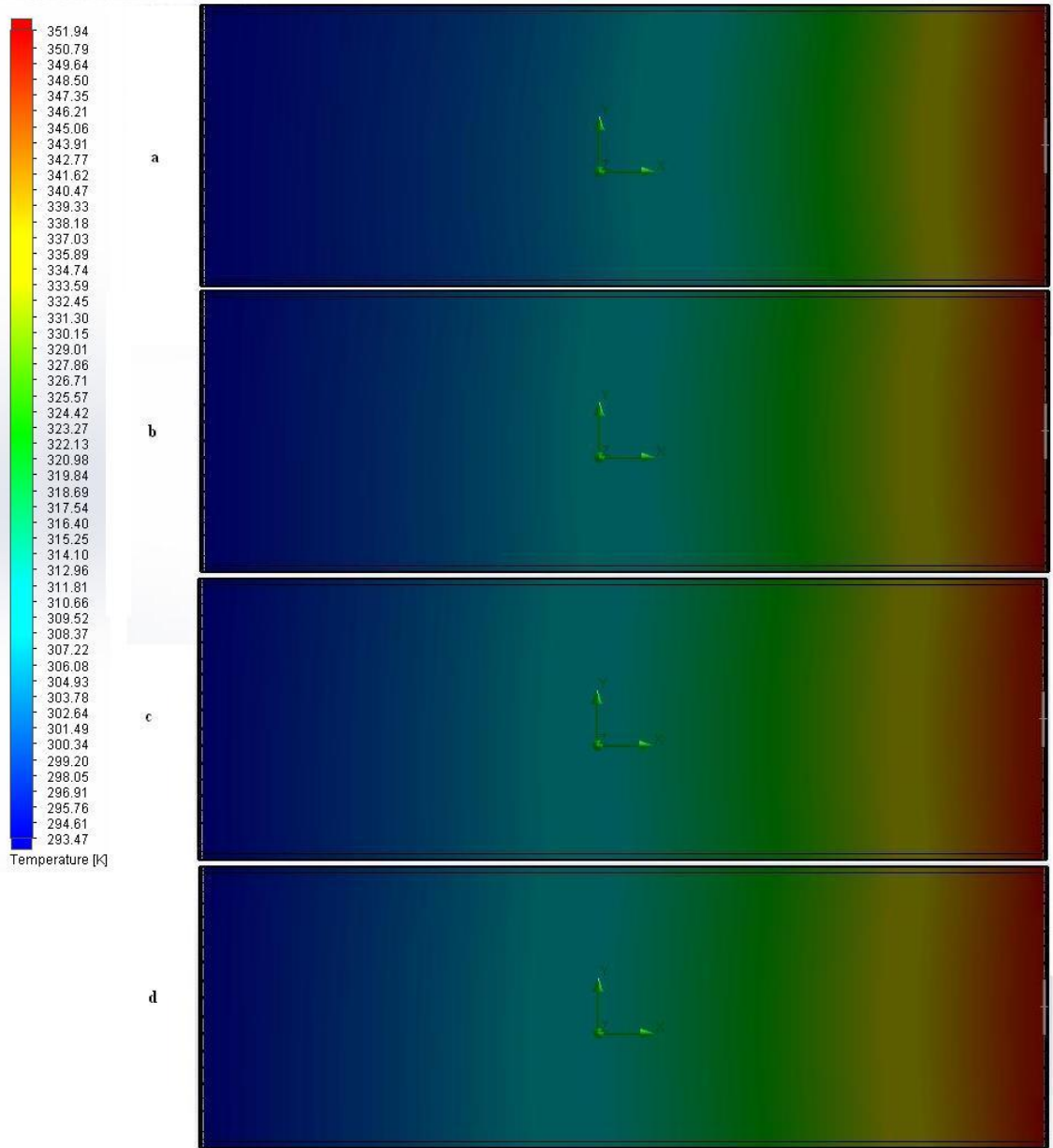


Figure 35. Temperature distribution cut plot at a) 900sec, b) 1800sec, c) 3600sec, and d) 7200s.

2. Condensation of electrolyte

Another issue discovered during testing was the condensation of the electrolyte with increasing testing time and temperature gradient. This effect was noticed for all testing cycles, configurations, and electrolyte concentrations. Electrolyte condensation

will change the thermocell performance for long running cycles. Water condensation will change the concentration of the electrolyte and thus lead to worse performance than expected.



Figure 36. Condensation of electrolyte during testing of 0.01M $\text{CuSO}_4 \cdot 5\text{H}_2\text{O}$ based thermocell.

Avoiding any air gaps in the thermocell design might help with the condensation of the electrolyte. So far no other reference study has reported issues or possible solutions for electrolyte condensation. From literature, however, the decomposition point for the tested $\text{CuSO}_4 \cdot 5\text{H}_2\text{O}$ is around $T = 110\text{ }^\circ\text{C}$ (Haynes, 2011). Hence, it is possible that the

electrolyte in the present study started to decompose even though hot electrode temperatures did not exceed $T = 90\text{ }^{\circ}\text{C}$. Fewer ions would be available for current flow and thus decrease the power output. For a commercial thermocell, designed to last for many years, this would be a disadvantageous electrolyte characteristic.

VII. CONCLUSION

The study presented provides a good foundation for the study and optimization of a Copper II Sulfate Pentahydrate based thermocell. Different design guidelines can be used to further study and improve thermogalvanic cells. Higher concentrations of $\text{CuSO}_4 \cdot 5\text{H}_2\text{O}$ will lead to better performance and very low concentrations are non-viable low energy sources due to the limited number of ions available. A threefold increase in concentration (from 0.1M to 0.3M) yielded around a threefold increase in maximum power production suggesting the relationship between electrolyte concentration and maximum power production is fairly linear.

Electrode separation also impacted maximum power production for a thermocell. It was shown that larger electrode spacing improved power production. Although the effect of increasing the electrode separation was not as profound as changing the electrolyte concentration, a doubling of electrode distance yielded around a one-third increase of the maximum power. Additionally, simulation results showed that there are more favorable heat effects for the $\text{CuSO}_4 \cdot 5\text{H}_2\text{O}$ when electrode are placed further apart. The temperature difference will be maintained more easily which will lead to better performance.

Another factor impacting the performance of a thermogalvanic cell was a change in electrode surface area. An increase in the surface area yielded a higher maximum power output. This change in maximum power was not as large as a change in

concentration. In fact, of all the changes made to the base thermocell, the change in electrode surface area had the smallest impact. The electrode surface area, however, should not be ignored in the design since for large scale applications appropriate changes can have a positive impact. It is also noteworthy that with a decrease in electrode surface area an increase in maximum power density and hence relative efficiency was measured. Thus for some applications a slight decrease in electrode surface area could increase the relative efficiency.

VIII. RECOMMENDATION

Future work should focus on the cyclic stability of the Copper II Sulfate Pentahydrate electrolyte. Only continuous use and very low maintenance will make this electrolyte useful for commercial applications. Thus electrode degradation and electrolyte condensation effects on power production should be investigated. Electrode deposits will prevent ion flow and thus lower the performance. Design options for condensation prevention need to be studied to ensure a constant electrolyte concentration for long cyclic stability.

This study showed that larger electrode separation will lead to better performance and higher maximum power. It is suspected that the linear relationship found for the electrode separation and increase in power production holds at all times due to aid of natural convection (Gunawan et al., 2014). Further testing with larger electrode separations would be necessary to find if this hypothesis is correct.

Another focus should lay on the mass transport overpotential which limits the ion flow. Having unsymmetrical electrode areas could free up more electrons for ion movement. Changing the surface areas of the hot and cold electrode could potentially lead to a power increase. Additionally, cheap additives to the $\text{CuSO}_4 \cdot 5\text{H}_2\text{O}$ electrolyte should be studied which could decrease the mass transport overpotential and increase ion flow.

REFERENCES

- Aseyev, I. D. Z. a. G. G. (1992). *Properties of Aqueous Solutions of Electrolytes* (1st Ed. ed.). Boca Raton, FL: CRC Press.
- Cadoff, I. B. M. E. (1960). *Thermoelectric Materials and Devices. [By various authors.] Edited by I.B. Cadoff ... and E. Miller ... Lectures presented during the course on Thermoelectric Materials and Devices ... New York University ... June 1959 and 1960.* Reinhold Pub. Corp.: New York; Chapman & Hall: London.
- Campbell, J. K. S., L.; Crooks, R. M. (1999). *Journal of American Chemical Society*, 121(3779).
- Crane, D., LaGrandeur, J., Jovovic, V., Ranalli, M., Adldinger, M., Poliquin, E., . . . Maranville, C. (2013). TEG On-Vehicle Performance and Model Validation and What It Means for Further TEG Development. *Journal of Electronic Materials*, 42(7), 1582-1591. doi: 10.1007/s11664-012-2327-8
- deBethune, A. J., Licht, T. S., & Swendeman, N. (1959). The Temperature Coefficients of Electrode Potentials: The Isothermal and Thermal Coefficients—The Standard Ionic Entropy of Electrochemical Transport of the Hydrogen Ion. *Journal of The Electrochemical Society*, 106(7), 616-625. doi: 10.1149/1.2427448
- Eastman, E. D. (1928). *Journal of American Chemical Society*, 50(292).
- Gunawan, A., Li, H., Lin, C.-H., Buttry, D. A., Mujica, V., Taylor, R. A., . . . Phelan, P. E. (2014). The amplifying effect of natural convection on power generation of thermogalvanic cells. *International Journal of Heat and Mass Transfer*, 78(0), 423-434. doi: <http://dx.doi.org/10.1016/j.ijheatmasstransfer.2014.07.007>
- Gunawan, A., Lin, C.-H., Buttry, D. A., Mujica, V., Taylor, R. A., Prasher, R. S., & Phelan, P. E. (2013). Liquid Thermoelectrics: Review of Recent And Limited New Data of Thermogalvanic Cell Experiments. *Nanoscale and Microscale Thermophysical Engineering*, 17(4), 304-323. doi: 10.1080/15567265.2013.776149
- Haynes, W. M. (2011). *CRC Handbook of Chemistry and Physics* (92nd ed. ed.). Boca Raton, FL: CRC Press.
- Ikeshoji, T., & Gonçalves, R. S. (1993). Thermogalvanic cells with aqueous redox couples and temperature differences larger than 100 K. *Journal of Applied Electrochemistry*, 23(5), 516-519. doi: 10.1007/BF00707631
- Kang, T. J., Fang, S., Kozlov, M. E., Haines, C. S., Li, N., Kim, Y. H., . . . Baughman, R. H. (2012). Electrical Power From Nanotube and Graphene Electrochemical Thermal Energy Harvesters. *Advanced Functional Materials*, 22(3), 477-489. doi: 10.1002/adfm.201101639

- Lee, H. (2010). *Thermal Design: Heat Sinks, Thermoelectrics, Heat Pipes, Compact Heat Exchangers, and Solar Cells*: Wiley.
- Mancini, T. H., P.; Butler, B. (2003). *Journal of Solar Energy Eng*, 125(135).
- Manda, S., Saini, A., Khaleeq, S., Patel, R., Usmani, B., Harinipriya, S., . . . Roy, B. (2013). Thermocells of carbon material electrodes and its performance characteristics. *Journal of Materials Research and Technology*, 2(2), 165-181. doi: <http://dx.doi.org/10.1016/j.jmrt.2013.01.005>
- Mua, Y., & Quickenden, T. I. (1996). Power Conversion Efficiency, Electrode Separation, and Overpotential in the Ferricyanide/Ferrocyanide Thermogalvanic Cell. *Journal of The Electrochemical Society*, 143(8), 2558-2564. doi: 10.1149/1.1837047
- Office of Energy Efficiency and Renewable Energy, V. T. P. (2004). *Energy Use, Loss, and Opportunities Analysis*. Oak Ridge National Laboratory, Oak Ridge Tennessee.
- Onsager, L. (1931). Reciprocal Relations in Irreversible Processes. I. *Physical Review*, 37(4), 405-426.
- Quickenden, T. I., & Mua, Y. (1995). A Review of Power Generation in Aqueous Thermogalvanic Cells. *Journal of The Electrochemical Society*, 142(11), 3985-3994. doi: 10.1149/1.2048446
- Quickenden, T. I., & Vernon, C. F. (1986). Thermogalvanic conversion of heat to electricity. *Solar Energy*, 36(1), 63-72. doi: [http://dx.doi.org/10.1016/0038-092X\(86\)90061-7](http://dx.doi.org/10.1016/0038-092X(86)90061-7)
- Randles, J. E. B., & Somerton, K. W. (1952). Kinetics of rapid electrode reactions. Part 3.-Electron exchange reactions. *Transactions of the Faraday Society*, 48(0), 937-950. doi: 10.1039/TF9524800937
- Ratkje, S. I., T. (1990). *Journal of Electrochemical Society*, 137, 2088.
- Rosi, F. D. (1968). Thermoelectricity and thermoelectric power generation. *Solid-State Electronics*, 11(9), 833-868. doi: [http://dx.doi.org/10.1016/0038-1101\(68\)90104-4](http://dx.doi.org/10.1016/0038-1101(68)90104-4)
- Rowe, D. M. (2006). *Thermoelectrics handbook : macro to nano*. Boca Raton: CRC/Taylor & Francis.
- Salazar, P., Kumar, S., & Cola, B. (2014). Design and optimization of thermo-electrochemical cells. *Journal of Applied Electrochemistry*, 44(2), 325-336. doi: 10.1007/s10800-013-0638-y
- Tester, J. W. (1992). Evaluation of thermogalvanic cells for the conversion of heat to electricity. *MIT Energy Lab*.
- U. Birkholz, E. G., U. Stohrer, K. Voss. (1988). *Conversion of waste exhaust heat in automobiles using FeSi₂ thermoelements*. Paper presented at the 7th Int. Conf. on Thermoelectrics, Arlington, TX.

APPENDICIES

NOMENCLATURE

A	=	electrode surface area (m^2)
d	=	electrode spacing (m)
F	=	Faraday's constant ($9.6485 * 10^4 \text{ K mol}^{-1}$)
I	=	current (A)
I_{sc}	=	short circuit current (A)
J_{sc}	=	short circuit current density (A m^{-2})
P	=	Power (W)
P_{max}	=	maximum Power (W)
\dot{Q}	=	rate of heat flow (W s^{-1})
R_{int}	=	internal resistance (Ω)
R_{ext}	=	external resistance (Ω)
S	=	entropy (J/K)
T	=	temperature (C)
ΔV	=	Potential difference (V)
V_{oc}	=	Open circuit voltage (V)
α	=	Seebeck coefficient (V K^{-1})
π	=	Peltier coefficient (A s^{-1})
σ	=	electrical conductivity (S m^{-1})
κ	=	thermal conductivity ($\text{W m}^{-1} \text{ K}^{-1}$)
η_{pc}	=	power conversion efficiency (%)
η_r	=	relative efficiency (%)
τ	=	Thomson coefficient (V K^{-1})

CURRICULUM VITAE

NAME: Steffen Krebs

ADDRESS: 200 Bracken Ct.
Frankfort, KY 40601

DOB: Biedenkopf, Hestia, Germany – April 21, 1991

EDUCATION & TRAINING:

B.S., Physics
Georgetown College
2009-13

M.S., Mechanical Engineering
University of Louisville
2013-15

AWARDS: Meritorious Winner, COMAP Math Modeling (2012)

Physics Honor Awards (2010, 2013)

PRESENTATIONS: Modeling Competition presentation at KYMMA (2012)